

NICER Magnetar Burst Catalog

CHE-YEN CHU ,¹ CHIN-PING HU ,¹ TERUAKI ENOTO ,^{2,3} GEORGE A. YOUNES ,^{4,5} ANDREA SANNA,⁶ SEBASTIEN GUILLOT ,⁷ RACHAEL STEWART ,⁸ ZAVEN ARZOUMANIAN,⁹ MATTHEW G. BARING ,¹⁰ MARLON L. BAUSE ,¹¹ TOLGA GÜVER ,^{12,13} WYNN C. G. HO ,¹⁴ CHRYSSA KOUVELIOTOU ,⁸ ALEX VAN KOOTEN ,⁸ ZORAWAR WADIASINGH ,^{15,16,17} AND KEITH C. GENDREAU⁹

¹Department of Physics, National Changhua University of Education, Changhua 500207, Taiwan

²Department of Physics, Kyoto University, Kitashirakawa Oiwake, Sakyo, Kyoto 606-8502, Japan

³RIKEN Center for Advanced Photonics (RAP), 2-1 Hirosawa, Wako, Saitama 351-0198, Japan

⁴Astrophysics Science Division, NASA Goddard Space Flight Center, Greenbelt, MD 20771, USA

⁵Center for Space Sciences and Technology, University of Maryland, Baltimore County, Baltimore, MD 21250, USA

⁶University of Cagliari, 09042, Monserrato, Sardinia, Italy

⁷Institut de Recherche en Astrophysique et Planétologie, UPS-OMP, CNRS, CNES, 9 avenue du Colonel Roche, BP 44346, Toulouse Cedex 4, 31028, France

⁸Department of Physics, The George Washington University, Washington, DC 20052, USA

⁹Astrophysics Science Division, NASA GSFC, 8800 Greenbelt Rd., Greenbelt, MD 20771, USA

¹⁰Department of Physics and Astronomy - MS 108, Rice University, 6100 Main Street, Houston, Texas 77251-1892, USA

¹¹Max Planck Institut für Radioastronomie, Auf dem Hügel 69, 53121 Bonn, Germany

¹²Istanbul University, Science Faculty, Department of Astronomy and Space Sciences, Beyazit, 34119, Istanbul, Turkey

¹³Istanbul University Observatory Research and Application Center, Istanbul University 34119, Istanbul Turkey

¹⁴Department of Physics and Astronomy, Haverford College, 370 Lancaster Avenue, Haverford, PA 19041, USA

¹⁵Department of Astronomy, University of Maryland, College Park, Maryland 20742, USA

¹⁶Astrophysics Science Division, NASA Goddard Space Flight Center, Greenbelt, MD 20771, USA

¹⁷Center for Research and Exploration in Space Science and Technology, NASA/GSFC, Greenbelt, Maryland 20771, USA

ABSTRACT

In this paper, we present a comprehensive catalog of short bursts from magnetars based on eight years of *NICER* observations. A total of 1130 bursts were identified, making this the largest magnetar burst catalog to date. The sample is dominated by SGR 1935+2154, which contributes 76% of all detected bursts. We analyzed burst durations, spectral properties, and their correlations across multiple sources. Bursts from SGR 1935+2154 exhibit significantly longer durations, with a mean of 317 ms, compared to a mean of 23 ms for bursts from other magnetars. Two μ s-scale bursts were detected for the first time, originating from 1E 1048.1–5937 and CXOU J010043.1–721134. Spectral analysis in the 0.5–8 keV range using both blackbody and power-law models shows that bursts with higher fluences have harder spectra. In contrast, correlations between burst duration and spectral parameters are weak or absent. This catalog provides a valuable dataset for studying magnetar short bursts, enabling future modeling efforts and improving our understanding of the diversity and physical mechanisms of magnetar bursts.

Keywords: stars: magnetars — X-rays: stars

1. INTRODUCTION

Magnetars are a class of neutron stars characterized by their extremely strong magnetic fields, often exceeding 10^{14} – 10^{15} G (Duncan & Thompson 1992). In the X-ray band, unlike rotation-powered pulsars, which typically show steady emission, magnetars are known for their highly variable and transient behavior (e.g., Coti Zelati et al. 2018). The first discovered magnetar burst was the giant flare from SGR 0526–66 in 1979, followed by

a short burst (Mazets et al. 1979b). Shortly afterwards, a series of short bursts was detected from SGR 1900+14 (Mazets et al. 1979a). Because these repeating events are dominated by emission in the soft γ -ray band, the sources were named soft gamma repeaters (SGRs). During a magnetar outburst, which can last from several months to several years, short bursts often appear in clusters known as burst forests or burst storms, with rates that can reach hundreds of bursts per hour (e.g.,

Younes et al. 2020; Hu et al. 2025). In contrast, during the quiescent state, bursts may appear individually (e.g., Gavril et al. 2002). According to the magnetar model, these bursts are generally thought to be triggered by cracks in the neutron star crust, induced by extreme magnetic stress (Duncan & Thompson 1992; Thompson & Duncan 1995).

With the discovery of more SGRs, several short-burst catalogs of individual sources have been reported, including SGR 1806–20, SGR 1900+14, 1E 1547.0–5408, SGR 0501+4516, etc. (Gögiş et al. 2001; van der Horst et al. 2012; Lin et al. 2013). Most of these studies focused on bursts in the hard X-ray band (>10 keV), while some extended to the soft X-ray range (<10 keV). The burst durations are typically log-normally distributed over more than two orders of magnitude, peaking around 200 ms. Their X-ray spectra can generally be described equally well by models such as a double blackbody, optically thin thermal bremsstrahlung, or a Comptonized model. A clear correlation between spectral hardness and brightness has been observed in these catalogs, where bursts with higher fluence tend to exhibit harder spectra, regardless of the adopted spectral model (Gögiş et al. 2001; van der Horst et al. 2012; Lin et al. 2013).

A more comprehensive burst catalog was later compiled using data from *Fermi*/Gamma-ray Burst Monitor (GBM), which included bursts from more than eight magnetar sources, though the majority originated from 1E 1547.0–5408 (Collazzi et al. 2015). The timing and spectral properties reported in this catalog are consistent with those obtained from earlier observations. In the 2020s, several magnetars underwent new outbursts that produced numerous short bursts. Detailed analyses have been conducted for bursts from Swift J1555.2–5402, SGR 1830–0645, and SGR 1935+2154 (Enoto et al. 2021; Younes et al. 2022; Hu et al. 2025). While their general properties are similar to those of other magnetar bursts, the events from SGR 1935+2154 stand out with substantially longer durations, peaking around 1 s, which is significantly longer than other magnetars (Younes et al. 2020).

The longer-duration short bursts were observed during the 2020 outburst of SGR 1935+2154. During this outburst, a fast radio burst (FRB) 20200428, was detected and confirmed to be associated with a short burst from SGR 1935+2154 (CHIME/FRB Collaboration et al. 2020; Bochenek et al. 2020; Mereghetti et al. 2020). This discovery established SGR 1935+2154 as the only Galactic magnetar known to emit FRBs. The FRB 20200428 associated X-ray short burst has a similar duration to other short bursts from this source (Li et al. 2021), however, its spectrum is significantly

softer (Younes et al. 2021). Beyond the distinctions seen within SGR 1935+2154 itself, Lin et al. (2013) reported systematic differences in duration distributions between magnetars. Together, these findings highlight the diversity of magnetar burst behavior, suggesting that physical conditions and emission mechanisms vary among sources and outbursts. A systematic comparison of bursts from multiple magnetars is therefore essential to constrain the physical origin and diversity of magnetar short bursts.

In this paper, we present a systematic study of magnetar short bursts using eight years of *Neutron Star Interior Composition Explorer (NICER)* observations. We compile a catalog of bursts from multiple magnetars, including the highly active SGR 1935+2154 as well as magnetar-like pulsars (Gavril et al. 2008; Archibald et al. 2016; Gögiş et al. 2016), and perform analysis of their timing and spectral properties. We also investigate correlations among these properties and explore variations between different sources. This comprehensive analysis provides a uniform catalog of magnetar short bursts observed by *NICER*, offering a resource for future modeling and theoretical studies.

2. DATA AND ANALYSIS

2.1. Data Selection and Reduction

NICER is a soft X-ray (0.2–12 keV) telescope mounted on the International Space Station (Gendreau et al. 2016). Its X-ray Timing Instrument (XTI) consists of 56 Focal Plane Modules (FPMs), though only 52 modules were in operation. While it does not offer imaging capability, *NICER* provides exceptionally high time resolution (~ 100 ns) and a large effective area, making it ideal for studying transient events. For this work, we selected all *NICER* observations conducted from its launch, 2017 June, through 2025 June 30 that included a magnetar or a magnetar-like pulsar within the field of view. Among the 26 known magnetars (Olausen & Kaspi 2014)¹, *NICER* has observed 21 of them, along with two additional magnetar-like pulsars. We collected 6016.9 ks of exposure time from 2765 *NICER* observations across 23 sources. The total exposure time and number of observations used for each source are summarized in Table 1.

We used HEASOFT version 6.34 (Nasa High Energy Astrophysics Science Archive Research Center (Heasarc) 2014) to reduce the *NICER* data. The standard calibration and screening were performed by the task `nicer12` with default options. The task `barycorr` was then ap-

¹ McGill Online Magnetar Catalog <http://www.physics.mcgill.ca/~pulsar/magnetar/main.html>

Table 1. *NICER* observations used for each magnetar and magnetar-like pulsar

Magnetars	Number of observations	Exposure (ks)
CXOU J010043.1–721134	241	725.0
4U 0142+61	166	330.0
SGR 0418+5729	16	21.3
SGR 0501+4516	198	498.9
1E 1048.1–5937	319	383.2
1E 1547.0–5408	60	87.9
Swift J1555.2–5402	68	118.1
PSR J1622–4950	22	46.0
CXOU J164710.2–455216	111	166.9
1RXS J170849.0–400910	113	84.9
CXOU J171405.7–381031	1	3.7
SGR J1745–2900	55	91.9
SGR 1806–20	15	37.2
XTE J1810–197	168	514.2
Swift J1818.0–1607	74	181.2
Swift J1822.3–1606	12	14.7
SGR 1830–0645	78	245.1
1E 1841–045	170	386.6
SGR 1900+14	1	0.4
SGR 1935+2154	415	1094.
1E 2259+586	149	179.7
PSR J1119–6127*	111	157.0
PSR J1846–0258*	202	648.9
Total	2765	6016.9

* Magnetar-like pulsars

plied with the JPLEPH.430 ephemeris to calibrate the time to Barycentric Dynamical Time (TDB). The resulting event lists were separated into the standard (0.5–8 keV) and high-energy (10–12 keV) bands for magnetar burst searches. On 2023 May 22, *NICER* sustained damage to its optical blocking film, leading to optical light leakage that degraded data quality. Observations taken after this date were processed separately. Nighttime data were reduced using the standard procedure described above. For daytime data, the `nicer12` task was executed with a screening option of `threshfilter=DAY` to account for increased optical contamination.

2.2. Burst Searching

We applied the Bayesian block algorithm to both the standard and high-energy event lists to identify significant flux variations (Scargle 1998). Blocks occurring during high-particle-background intervals, as defined by the high-energy band, were excluded. In the standard band, blocks with durations shorter than 1 s were se-

Table 2. Details of *NICER* observations on *RXTE* blank sky regions after excluding high-background intervals

Sky region	ObsID	Exposure (ks)	Counts
RXTE1	6012010106	3.1	1916
RXTE2	1012020169	18.6	6924
RXTE3	1012030123	5.3	2812
RXTE4	5012040217	8.3	4336
RXTE5	1012050131	5.8	4234
RXTE6	4012060255	13.3	7400
RXTE8	1012080190	12.2	5574

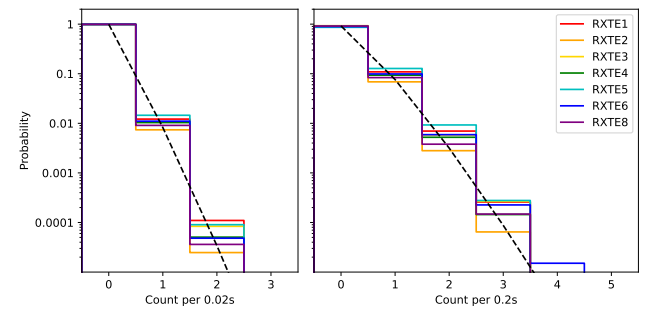


Figure 1. Distributions of background counts calculated with 0.02 s (left) and 0.2 s (right) time bins. Different colors correspond to the RXTE blank-sky regions identified in the legend. Black dashed lines are the Poisson probability mass function of averaged background counts calculated from Table 2.

lected as burst candidates. We further examined the FPM distribution of each candidate. Candidates with events concentrated in only one or two FPMs were identified as particle-induced events and excluded from the burst sample.

For each burst candidate, we estimated the statistical significance by computing the Poisson probability of detecting the observed number of counts within the burst block. A nearby interval of ≤ 5 s was selected to represent the non-burst count rate. After accounting for the number of trials, we retained only those blocks with a Poisson probability less than 10^{-5} for further analysis. The number of trials was defined as the total exposure time of each observation divided by 0.2 s, which is a typical magnetar burst duration (Collazzi et al. 2015).

NICER has been monitoring seven X-ray blank regions defined initially by the *Rossi X-ray Timing Explorer* (*RXTE*; Jahoda et al. 2006). We selected one observation from each region and excluded intervals with high particle background. The details of the blank sky observations used are summarized in Table 2. We binned the cleaned event lists into 0.2 s and 0.02 s bins, matching the burst durations reported in previous work (Col-

Table 3. Total number of short bursts found from each magnetar in the *NICER* dataset.

Magnetars	Number of burst
CXOU J010043.1–721134	4
4U 0142+61	4
SGR 0418+5729	0
SGR 0501+4516	0
1E 1048.1–5937	1
1E 1547.0–5408	0
Swift J1555.2–5402	74
PSR J1622–4950	0
CXOU J164710.2–455216	0
1RXS J170849.0–400910	1
CXOU J171405.7–381031	0
SGR J1745–2900	0
SGR 1806–20	4
XTE J1810–197	1
Swift J1818.0–1607	27
Swift J1822.3–1606	1
SGR 1830–0645	128
1E 1841–045	15
SGR 1900+14	0
SGR 1935+2154	865
1E 2259+586	1
PSR J1119–6127*	0
PSR J1846–0258*	4
Total	1130

* Magnetar-like pulsars

lazzi et al. 2015) as well as those found in this study. We then recorded the total counts in each bin to characterize the background X-ray distribution. The cumulative distribution function reaches 100% at 4 counts per 0.2 s bin and 3 counts per 0.02 s bin (Figure 1). To ensure robust separation between genuine bursts and background fluctuations, we required that a burst candidate contain at least 5 counts within a Bayesian block. Based on the measured background rate and the *NICER* effective area, the expected detection limits for a transient event are approximately 2 and 2.5×10^{-11} erg s $^{-1}$ cm $^{-2}$ for transient duration 0.02 s and 0.2 s respectively.

2.3. Analysis

We first plotted the cumulative counts of each selected burst, after subtracting the non-burst count rate, and fitted the resulting curve with a step function (Görgüç et al. 2001). The step height corresponds to the total number of counts in the burst. This total count was then used to compute the 5% and 95% levels of the cumulative distribution. The time interval between when the cumulative count reaches 5% and 95% is defined as

the T_{90} duration (Kouveliotou et al. 1993). For bursts with fewer than 20 total counts, the 5% fractional level corresponds to less than one count, making T_{90} not accurately defined. In these cases, T_{90} is instead defined as the duration of the corresponding Bayesian block.

The Bayesian blocks interval of each burst defines its good time interval (GTI), and the counts within this GTI were used for the spectral analysis. We first calculated the hardness ratio (HR), defined as

$$HR = \frac{\text{hard} - \text{soft}}{\text{hard} + \text{soft}}, \quad (1)$$

where *soft* denotes photons in the 0.5–4 keV range and *hard* denotes photons in the 4–8 keV range. Some bursts show no photons below 2 keV because of strong absorption along the line of sight, so we adopted 4 keV as the boundary between the soft and hard photons, rather than 2 keV.

We also extracted 0.5–8 keV burst spectra from the burst GTI with the task `nicerl3-spect` and performed spectral fitting using `XSPEC` v12.14 (Nasa High Energy Astrophysics Science Archive Research Center (Heasarc) 2014). The non-burst interval used for estimating the burst significance was also adopted as the background spectrum for subtraction during fitting. The spectra were binned according to the total number of burst counts: for bursts with fewer than 20 counts, at least 1 count per bin; for 20–49 counts, each bin contained at least 5 counts; for 50–249 counts, at least 10 counts per bin; and for more than 250 counts, at least 25 counts per bin. Each burst spectrum was fitted with both a blackbody and a power-law model. In all fits, the hydrogen column density (n_H) was fixed to values reported in the literature for each of the magnetars (Chu & Chang 2023; Enoto et al. 2021; Borghese et al. 2021; Hu et al. 2020; Younes et al. 2022; Hu et al. 2023). For bursts with fewer than 20 total counts, the blackbody temperature (kT) or the power-law photon index (Γ) was also fixed at 1.2 keV and 0.8, respectively. The `cstat` in the `XSPEC` statistic was used for bursts with fewer than 250 counts, while the `chi` statistic was adopted for bursts with 250 counts or more. Once the best-fit parameters were obtained, we calculated the absorbed flux for both models in the 0.5–10 keV range. All uncertainties reported in this paper correspond to 1σ confidence levels.

3. RESULTS AND DISCUSSION

3.1. Overall samples

We detected a total of 1130 bursts in our dataset, including four from the magnetar-like pulsar PSR J1846–0258. The majority of events (76.5%) originated from SGR 1935+2154, which has been the most

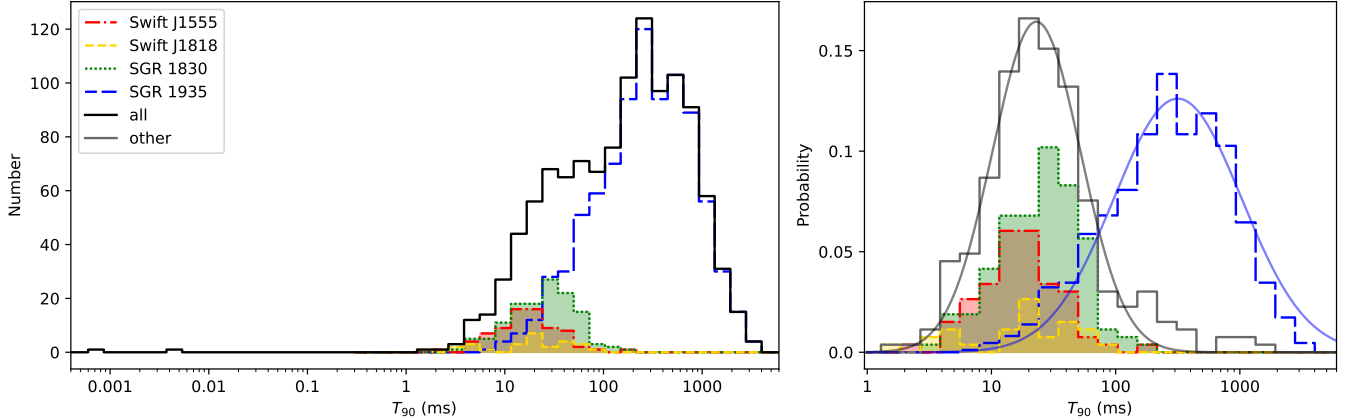


Figure 2. The left panel shows the overall duration distribution of the NICER magnetar bursts, and the right panel focuses on bursts with durations longer than 1 ms. In the right panel, the sample is divided into two groups: SGR 1935+2154 and all other magnetars, with each distribution normalized by its respective sample size so that their histogram sums to 1. The Red dash-dotted line represents Swift J1555.2–5402 (Swift J1555), the yellow dashed line represents Swift J1818.0–1607 (Swift J1818), and the green dotted line represents SGR 1830–0645 (SGR 1830). The histograms of these three samples are filled for clarity. The blue long-dashed line corresponds to SGR 1935+2154 (SGR 1935), and the black solid histogram represents all bursts. The gray histogram shows all samples except SGR 1935+2154. The blue and the gray curves indicate the log-normal fits to the normalized SGR 1935+2154 and other samples, respectively.

active magnetar in recent years. *NICER* captured its major outbursts in April 2020, September 2021, and October 2022 (Younes et al. 2020; Güver et al. 2021; Hu et al. 2025), during which some Galactic FRBs were also observed (CHIME/FRB Collaboration et al. 2020; Bochenek et al. 2020; Kirsten et al. 2021; Dong & Chime/Frb Collaboration 2022; Giri et al. 2023).

Several magnetar outbursts have also been captured by *NICER* since its launch in 2017 June, including the 2020 outburst of Swift J1818.0–1607 (Hu et al. 2020), the 2020 outburst of SGR 1830–0645 (Younes et al. 2022), the 2021 outburst of Swift J1555.2–5402 (Enoto et al. 2021), and the 2024 outburst of 1E 1841–045 (Younes et al. 2025). These sources accounted for 21.6% of the bursts in our sample. *NICER* also observed additional outbursts from other magnetars, such as XTE J1810–197 (Güver et al. 2019), and PSR J1846–0258 (Hu et al. 2023). However, in these cases, the outburst activity was relatively weak or the observations did not coincide with the outburst onset, resulting in fewer detected bursts.

The number of bursts detected from each source is summarized in Table 3, while details of individual bursts are provided in Appendix A. Several of these bursts have also been reported in earlier studies focused on individual sources, and here we place them in the broader context of the *NICER* magnetar sample.

3.2. T_{90} duration

The distribution of T_{90} durations for all bursts is shown in Figure 2. The overall sample has a mean

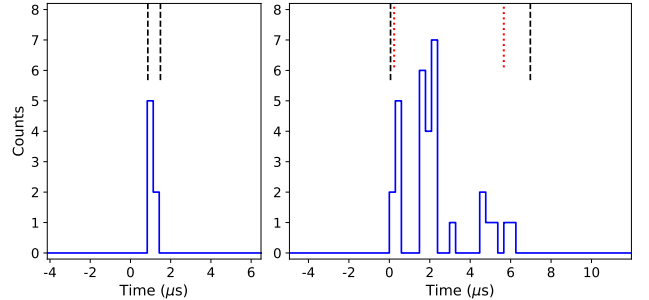


Figure 3. Light curves of the μ s-scale bursts with 0.3μ s time bins. The left panel shows the burst with a T_{90} of 0.6μ s, with the zero point at 2018-11-22T11:58:14.425441 (TDB). The right panel shows the burst with a T_{90} of 5μ s, with the zero point at 2022-07-24T23:59:07.273212 (TDB). The black vertical dashed lines indicate the Bayesian block boundaries, and the red dotted lines mark the calculated T_{90} intervals.

T_{90} of 350 ms and a standard deviation of 470 ms. Two μ s-scale bursts were identified in our sample: one from 1E 1048.1–5937 with a duration of 0.6μ s, and another from CXOU J010043.1–721134 with a duration of 5μ s. These represent the first detections of μ s-scale bursts in X-rays from magnetars. Their light curves are shown in Figure 3. Since no sub-ms bursts were found, it remains unclear whether these events are simply the extreme tail of the main burst distribution or instead represent a distinct class of magnetar short bursts. Future X-ray missions with larger effective area will be crucial to resolve this question.

Table 4. Log-normal fitting results to T_{90} duration distributions from different magnetar groups and studies.

Magnetars	Instrument	peak (ms)	16–84% quantile (ms)
SGR 1935+2154	<i>NICER</i> /XTI	317	95–1026
Other magnetars	<i>NICER</i> /XTI	23	10–52
SGR 1935+2154 ¹	<i>NICER</i> /XTI	840	430–1630
1E 1547.0–5408 ²	<i>Swift</i> /XRT	207	62–685
1E 1547.0–5408 ³	<i>Fermi</i> /GBM	156	62–389

References. (1) Younes et al. (2020) (2) Lin et al. (2013)
(3) Collazzi et al. (2015)

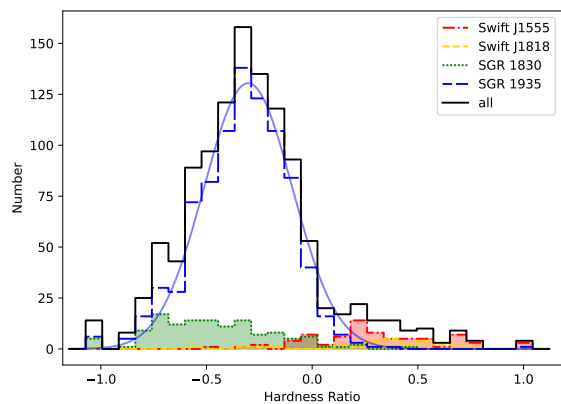


Figure 4. Hardness ratio distribution of all bursts. Different histograms represent magnetar groups as defined in Figure 2 and indicated in the legend. The blue curve shows the normal distribution fit to the SGR 1935+2154 sample.

Bursts from SGR 1935+2154 exhibit T_{90} values that are significantly longer than those of other magnetars. We fitted log-normal distributions to both groups and show the normalized distributions in Figure 2. For SGR 1935+2154, the distribution peaks at 316 ms, while it peaks at 23 ms for the remaining magnetars. Thus, bursts from SGR 1935+2154 are on average about an order of magnitude longer. A Kolmogorov–Smirnov (KS) test applied to the two distributions yields a probability of 3.5×10^{-106} , confirming that the two samples are distinct.

Younes et al. (2020) studied bursts from SGR 1935+2154 during its 2020 outburst using *NICER* data. These events are also included in our sample, accounting for roughly 40% of the SGR 1935+2154 bursts analyzed here. However, the T_{90} durations we obtain are systematically shorter than those reported in Younes et al. (2020). A key reason is the different treatment of multi-peak bursts: we apply a 0.2 s

criterion to decide whether peaks belong to separate bursts, whereas their study used 0.5 s. Consequently, they classified more events as multi-peak bursts, yielding shorter durations if treated as individual bursts. A second factor is the difference in burst populations across epochs. *NICER* captured a burst storm from SGR 1935+2154 in the 2020 outburst, during which the persistent emission was higher than usual. Dim or very short bursts may have been buried in this elevated background and thus missed. In contrast, the bursts detected in the 2021 and 2022 outbursts occurred during lower persistent-emission states, making weaker and shorter events easier to identify. As a result, the 2021 and 2022 bursts exhibit shorter duration distributions overall, pulling the combined distribution toward smaller T_{90} values.

Regardless of methodology, the burst durations of SGR 1935+2154 differ significantly from those of other magnetars, suggesting possible intrinsic differences between this source and the broader magnetar population. SGR 1935+2154 is currently the only Galactic magnetar known to produce FRBs (CHIME/FRB Collaboration et al. 2020; Bochenek et al. 2020), and numerous studies have explored what physical mechanisms might make it distinct. Hu et al. (2025) reported that during the 2022 outburst of SGR 1935+2154, the burst properties evolved across different epochs, with a notable change after an intermediate flare. The X-ray bursts that occurred after the flare, including those around the time of FRB 20221014A (Dong & Chime/Frb Collaboration 2022), exhibit properties that differ significantly from the pre-flare burst population. Younes et al. (2021) also found that the X-ray counterpart of FRB 20200428 exhibited a softer spectrum compared to typical bursts, potentially indicating an origin in a different region of the magnetosphere.

These findings suggest that the differences in T_{90} durations between SGR 1935+2154 and other magnetars may reflect variations in the burst mechanism across different outbursts and even between epochs within a single outburst. Our SGR 1935+2154 sample combines bursts from the 2020, 2021, and 2022 outbursts, and further disentangling these epoch-dependent effects will be necessary to understand the underlying physics. A detailed comparison of burst properties across different epochs of SGR 1935+2154 will be presented in a forthcoming paper (Chu et al., in preparation). Together, these results emphasize that SGR 1935+2154 is an exceptional case among magnetars, potentially connected to its unique ability to produce FRBs.

In addition to bursts from other magnetars, Lin et al. (2013) reported 275 bursts from 1E 1547.0–5408 de-

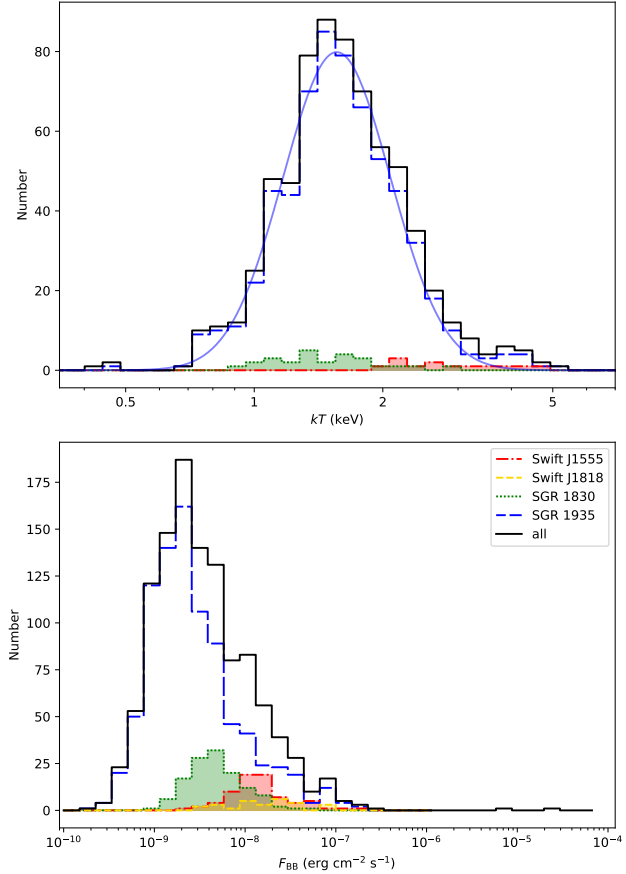


Figure 5. Blackbody temperature kT (top) and flux F_{BB} (bottom) distributions of all bursts. Different histograms represent magnetar groups as defined in Figure 2 and indicated in the legend. For the kT distribution, most Swift J1818.0–1607 bursts have fewer than 20 counts, and their kT values were fixed during spectral fitting; therefore, this sample is not plotted separately on the top panel.

ected with *Swift*/X-ray Telescope (XRT), with a T_{90} distribution peaking at 207 ms and 262 bursts from SGR 0501+4516 detected with *XMM-Newton*, whose T_{90} durations peak at about 100 ms. Collazzi et al. (2015) presented a catalog of 440 bursts from at least eight magnetars observed by *Fermi*/GBM. Among these, 386 bursts originate from 1E 1547.0–5048 and have a T_{90} peak at 156 ms, while the remaining bursts peak around 80 ms. Overall, these duration distributions are longer than those of the regular magnetar bursts in our *NICER* sample. Because *NICER* offers superior time resolution and larger effective area than those aforementioned missions, it is more sensitive to faint or shorter duration bursts. As a result, our catalog contains many more short events, leading to systematically shorter T_{90} distributions compared to previous studies. A summary of the log-normal fitting results

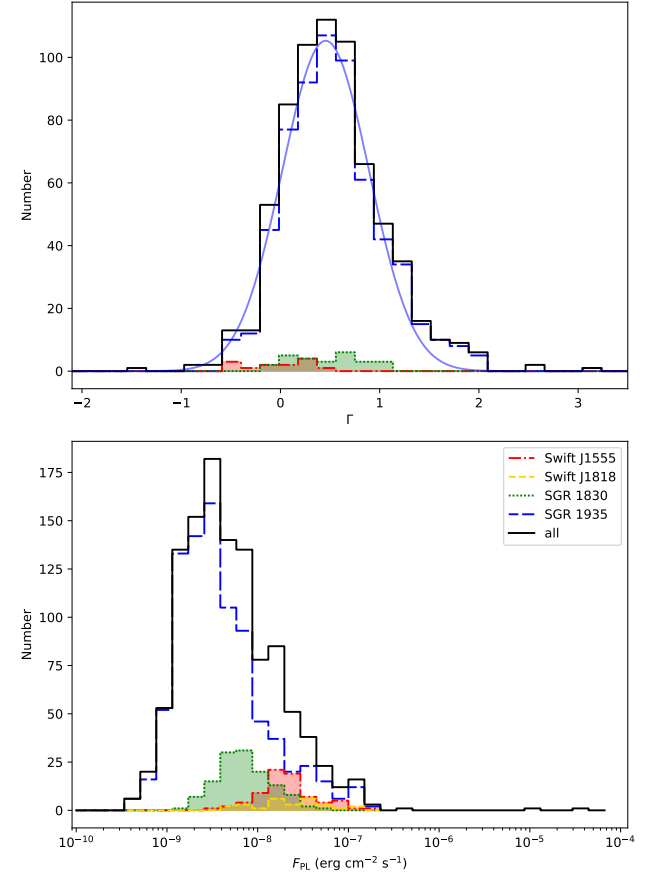


Figure 6. Power index Γ (top) and flux F_{PL} (bottom) distributions of all bursts. Different histograms represent magnetar groups as defined in Figure 2 and indicated in the legend. For the Γ distribution, most Swift J1818.0–1607 bursts have fixed Γ values during spectral fitting; therefore, this sample is not plotted separately on the top panel.

of the T_{90} distributions, including the peak values and 16–84% quantile ranges for different groups and instruments, is presented in Table 4.

3.3. Hardness ratio

The distribution of the HR is shown in Figure 4. The overall distribution has a mean of -0.29 and a standard deviation of 0.31. Most bursts exhibit relatively soft spectra, while those from Swift J1555.2–5402 and Swift J1818.0–1607 are noticeably harder, with HR mostly greater than zero. This trend is consistent with the higher column densities of these sources ($n_H = 8.72$ and 11.2×10^{22} atoms cm^{-2} , respectively), which preferentially absorb more soft photons compared to other magnetars.

For SGR 1935+2154, the HR distribution is well described by a normal distribution with a mean of -0.30 and a standard deviation of 0.21. This distribution is

similar to those of other low- n_H magnetars, in contrast to the marked differences observed in their burst-duration distributions.

3.4. Spectral model

The spectra of magnetar bursts in the soft X-ray band can be equally well described by either a single power-law or a single blackbody model (e.g., Kirmizibayrak et al. 2017). Therefore, each burst spectrum was fitted individually with both models to account for both possibilities.

The results of the blackbody fits are shown in Figure 5, which presents the distributions of blackbody temperature (kT) and flux (F_{BB}). Fitting the kT distribution of SGR 1935+2154 group with a log-normal function yields a peak at 1.56 keV and a 16–84% quantile range of 1.17–2.08 keV. This characteristic temperature is slightly lower than that obtained from *Swift*/XRT bursts of 1E 1547.0–5408 (~ 2.5 keV; Lin et al. 2013) and considerably lower than that of *Fermi*/GBM bursts (~ 4.5 keV; Collazzi et al. 2015). The difference likely reflects *NICER*’s higher sensitivity to fainter bursts, which tend to exhibit softer spectra (Gögiş et al. 2001; Lin et al. 2013), corresponding to lower blackbody temperatures (see also Section 3.5). As a result, the inclusion of additional dim bursts shifts the overall kT distribution toward lower values. The higher temperatures inferred from *Fermi*/GBM may also arise because those fits correspond to the lower-temperature component of a two-blackbody model in the 8–200 keV range, where the cooler component is poorly constrained and thus biased upward. Alternatively, the broadband spectra may be better represented by three blackbody components rather than two. In any case, the burst temperatures are significantly higher than the typical magnetar temperature in quiescence of ~ 0.45 keV (Chu & Chang 2023), and even during the onset of outburst of ~ 0.8 keV (e.g. Gotthelf et al. 2019). The fluxes are generally distributed between 10^{-10} and 3×10^{-7} $\text{erg s}^{-1} \text{cm}^{-2}$, with the two μs -scale bursts showing much higher fluxes of $\sim 10^{-5}$ $\text{erg s}^{-1} \text{cm}^{-2}$.

The results of the power-law spectral fits are shown in Figure 6, which display the distributions of photon index (Γ) and corresponding flux (F_{PL}). A normal distribution fit to SGR 1935+2154 group yields a mean Γ of 0.45 and a standard deviation of 0.44. Overall, the burst spectra are systematically harder than those of the magnetars persistent emission in quiescence. The flux distribution obtained from the power-law model is broadly consistent with that derived from the blackbody model, indicating that the inferred burst fluxes are not strongly dependent on the chosen spectral model.

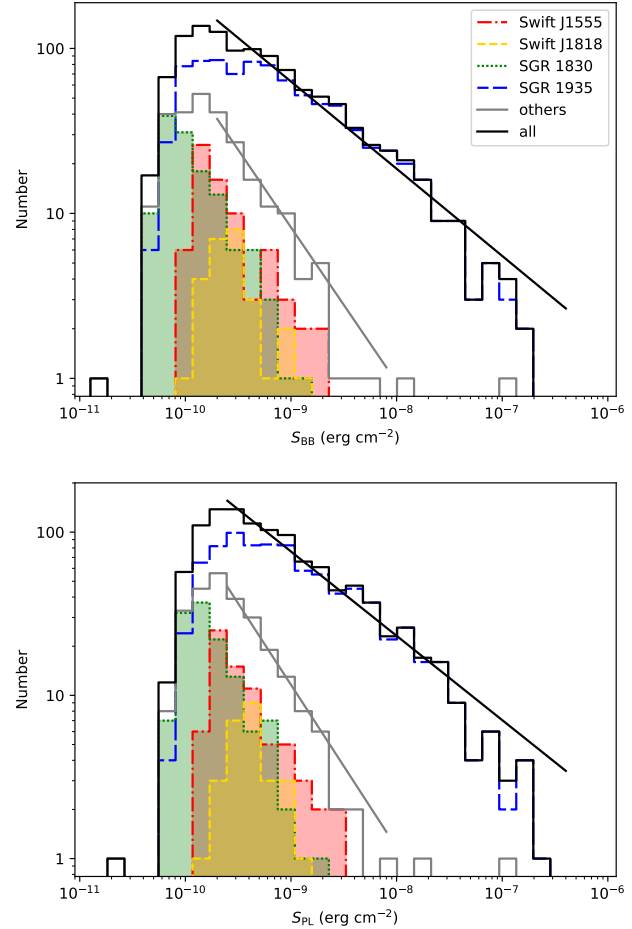


Figure 7. Fluence distributions derived from the blackbody model S_{BB} (top) and the power-law model S_{PL} (bottom) for all bursts. Different histograms represent magnetar groups as defined in Figure 2 and indicated in the legend. The black lines show the best-fit power-law functions for the full burst sample, with indices of -0.53 ± 0.04 for the blackbody model and -0.52 ± 0.03 for the power-law model. The gray lines show the best-fit power-law functions for the sample excluding SGR 1935+2154, with indices of -0.94 ± 0.06 and -1.00 ± 0.06 for the two spectral models.

The fluence (S_{BB} and S_{PL}) distributions, calculated from the fluxes and T_{90} durations, for both the blackbody and power-law models are shown in Figure 7 as $\log(S)$ – $\log(N)$ plots. For fluences above 2×10^{-10} erg cm^{-2} , the distributions are well described by power-laws, yielding indices of -0.53 ± 0.04 for the blackbody model and -0.52 ± 0.03 for the power-law model. Because the full sample is dominated by SGR 1935+2154, we also fit the distributions after excluding its bursts. This yields significantly steeper slopes of -0.94 ± 0.06 for the blackbody and -1.00 ± 0.06 for the power-law model. These results demonstrate that SGR 1935+2154 exhibits a distinct fluence distri-

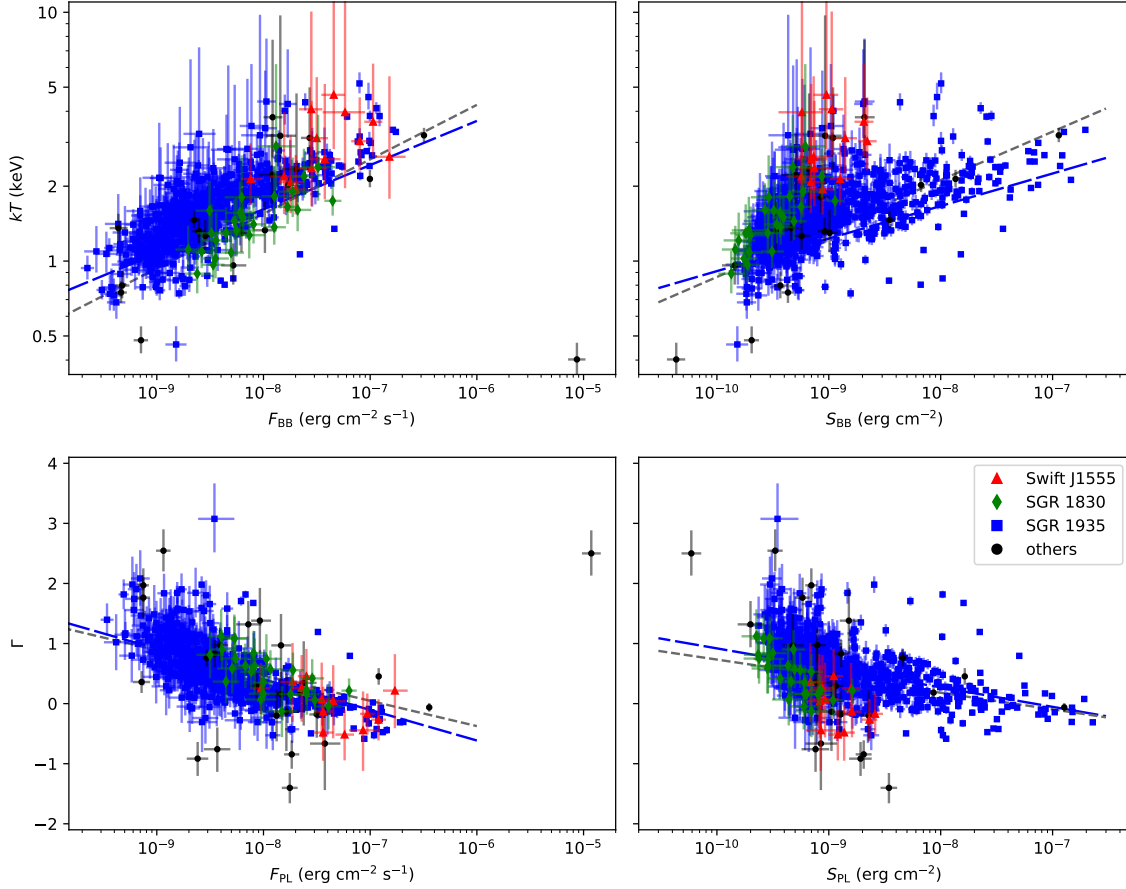


Figure 8. Distribution of spectral parameters of all bursts. The red triangles represent Swift J1555.2–5402, the green diamonds represent SGR 1830–0645, the blue squares represent SGR 1935+2154, and the black circles represent the remaining magnetars. The blue long-dashed lines and the gray dashed lines show the best-fit power-law relations for SGR 1935+2154 and for all other magnetars, respectively.

bution compared to other magnetars. Its longer burst durations lead to a larger number of high-fluence events, which strongly influences the overall distribution.

From the turnover in these distributions, we estimate that *NICER* achieves nearly 100% detection efficiency above 2×10^{-10} erg cm $^{-2}$, with a detection limit of approximately 4×10^{-11} erg cm $^{-2}$. For the duration distribution of our burst sample, this detection limit is slightly higher than the expected value of 2.5×10^{-11} erg cm $^{-2}$ estimated in Section 2.2. The reason is that most of the bursts identified in this work occurred during a magnetar X-ray outburst, where the persistent emission is higher. As a result, the background level is higher, and some low-fluence bursts are buried in the background.

3.5. Correlation

The left panels of Figure 8 show the distributions of kT and Γ versus their corresponding fluxes. For low-count bursts, where kT or Γ were fixed during fitting, these points are not included in the figure. Overall,

bursts with higher fluxes tend to exhibit harder spectra, characterized by higher temperatures or smaller photon indices, consistent with previous studies (see, e.g., Göğüş et al. 2001; Lin et al. 2013). To quantify this relation, we calculated Pearson correlation coefficients (Pearson r) for bursts from SGR 1935+2154 and from other magnetars separately. The clear outlier, the 5 μ s burst from CXOU J010043.1–721134, was excluded from this analysis.

For SGR 1935+2154, the coefficients are 0.754 for kT versus F_{BB} and -0.702 for Γ versus F_{PL} . For the other magnetar bursts, the corresponding values are 0.807 and -0.556 , respectively. Strong correlations are found in all cases, except for the weaker Γ - F_{PL} relation in the other magnetar sample. We fitted power-law functions to these highly correlated relations, obtaining indices of 0.18 ± 0.01 and 0.22 ± 0.02 for SGR 1935+2154 and the other magnetars, respectively, for the kT - F_{BB} relation. For the Γ - F_{PL} relation, the indices are -0.51 ± 0.03 for SGR 1935+2154 and -0.42 ± 0.08 for the remaining

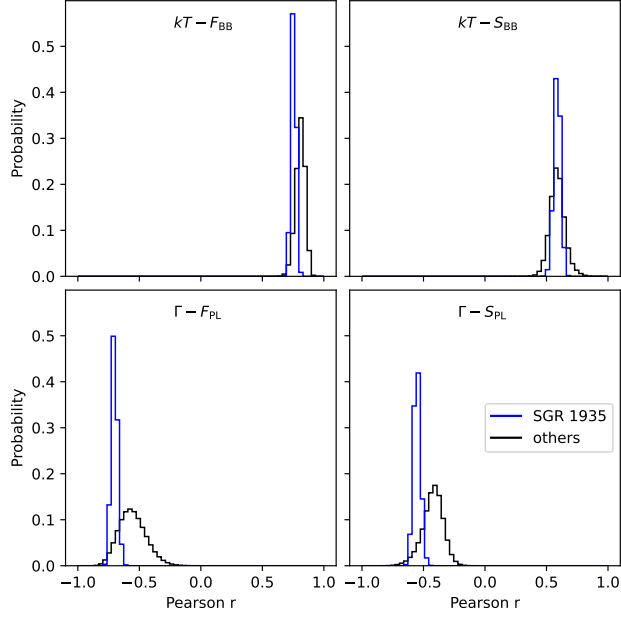


Figure 9. Distributions of Pearson correlation coefficients between spectral parameters obtained using the bootstrap method. The parameter combinations are indicated at the top of each panel. The blue and the black histograms represent the SGR 1935+2154 sample and all other magnetar samples, respectively.

magnetars. In addition to the μ s burst, two other events exhibit notably soft spectra ($kT < 0.5$ keV or $\Gamma > 2.5$): one from SGR 1935+2154 and one from 4U 0142+61.

The right panels of Figure 8 show the distributions of kT and Γ versus S_{BB} and S_{PL} , respectively. Similar to the flux relations, bursts with higher fluences generally exhibit harder spectra. For SGR 1935+2154, the Pearson correlation coefficients are 0.588 for kT versus S_{BB} and -0.554 for Γ versus S_{PL} , while for the other magnetar bursts, they are 0.574 and -0.411 , respectively. The correlations weaken when moving from flux to fluence, as the scatter increases at higher fluences, suggesting the presence of possible subgroups. However, after incorporating the duration parameter, the 5μ s burst aligns with the overall trend, remaining consistent with the main burst population.

We also examined the fluence relations using power-law fits. For the kT - S_{BB} relation, the derived indices are 0.13 ± 0.01 for SGR 1935+2154 and 0.19 ± 0.02 for the other magnetars. In the Γ - S_{PL} relation, the indices are -0.32 ± 0.03 for SGR 1935+2154 and -0.28 ± 0.07 for the remaining sources. Because these fits are driven primarily by the high-fluence end of the distribution, the results appear weaker and less well defined than those seen in the flux relations.

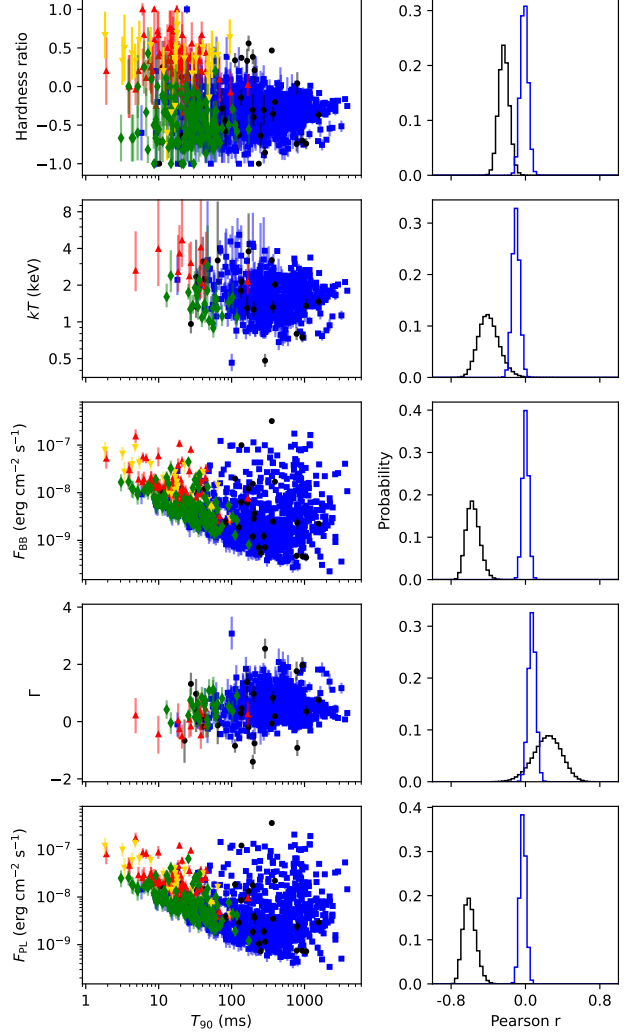


Figure 10. Distributions of T_{90} versus spectral parameters for all bursts (left panels) and the corresponding distributions of Pearson correlation coefficients obtained using the bootstrap method (right panels). Data points in the left panels represent magnetar groups as defined in Figure 8, with the yellow triangles indicating Swift J1818.0-1607. The blue and the black histograms in the right panels correspond to the SGR 1935+2154 sample and all other magnetars, respectively. The two μ s-scale bursts are excluded from this correlation analysis.

To further investigate possible subgroups within our sample, we performed a bootstrap analysis of the spectral correlations. For each selected burst sample, we generated a resampled dataset by randomly selecting bursts from the original sample until the resampled dataset matched the original in size. Each burst could be selected multiple times. We then recalculated the Pearson correlation coefficient for each resampled dataset. This process was repeated one million times, and the result-

ing distributions of correlation coefficients are shown in Figure 9.

The mean correlation coefficients derived from the bootstrap analysis are consistent with those obtained from the original samples across all parameter combinations. However, the coefficient distributions for the other magnetar bursts are noticeably broader than those for the SGR 1935+2154 sample, particularly for the power-law model. This wider spread likely reflects the inclusion of bursts from multiple magnetars, whose spectral parameters may be influenced by instrumental limitations and varying absorption along different lines of sight. The bootstrap results show no additional outlying behavior, and no secondary clusters or anomalous distributions appear across the one million trials. This suggests that all bursts follow a similar trend, except for the 5 μ s burst in the flux relation.

The correlations between burst duration and spectral parameters are shown in Figure 10, along with their bootstrap distributions. As with the spectral-spectral relations, bursts were divided into two groups: SGR 1935+2154 and all other magnetars. The two μ s-scale bursts were excluded from the analysis. For SGR 1935+2154, all correlations between T_{90} and the spectral parameters are statistically insignificant, with Pearson coefficients consistent with zero. This is consistent with earlier studies of magnetar bursts, which also found no clear correlation between timing and spectral properties (van der Horst et al. 2012).

In contrast, for the other magnetars, both F_{BB} and F_{PL} show an apparent anti-correlation with T_{90} . This trend is not intrinsic but instead results from instrumental limitations. Bursts with lower fluence are more likely to fall below the detection threshold, truncating the intrinsic burst population. The observed anti-correlation is therefore a selection effect. Similarly, the weak correlations and anti-correlations between T_{90} and spectral hardness, represented by HR, kT , and Γ , can be explained by the same detection bias. Shorter bursts tend to have lower fluxes, and as shown in Figure 9, fainter bursts generally display softer spectra. This leads to the weak correlations between duration and spectral parameters observed here.

4. SUMMARY

In this study, we constructed a comprehensive catalog of magnetar short bursts spanning eight years of *NICER* observations. We identified a total of 1130 bursts, making this the largest burst catalog to date. Most of the bursts originated from SGR 1935+2154, which contributed 865 events. We present the distributions of timing and spectral parameters for all de-

tected bursts and investigate their correlations. The bursts from SGR 1935+2154 generally show longer T_{90} durations than those from other magnetars. We also report the first detection of μ s-scale bursts in magnetars, one from 1E 1048.1–5937 and another from CXOU J010043.1–721134.

Bursts with higher fluxes tend to exhibit harder spectra, indicating higher blackbody temperatures in the blackbody model or lower photon indices in the power-law model. The bootstrap resampling analysis confirms that these spectral correlations are statistically robust, while correlations between burst duration and spectral parameters remain weak or absent. The weaker correlations found among other magnetars likely reflect differences in source properties and instrumental effects.

This catalog provides a uniform, statistically rich sample that will serve as a foundation for future investigations of magnetar burst energetics, emission mechanisms, and magnetic field dynamics.

¹ This research has made use of data and software provided by the High Energy Astrophysics Science Archive Research Center (HEASARC), which is a service of the Astrophysics Science Division at NASA/GSFC. C.-Y.C. acknowledges support from the National Science and Technology Council (NSTC) in Taiwan through grant 113-2811-M-018-003-MY2. C.-P.H. acknowledges support from the NSTC in Taiwan through grant 112-2112-M-018-004-MY3. S.G. acknowledges the support of the CNES.

Facilities: *NICER*

Software: Heasoft (Nasa High Energy Astrophysics Science Archive Research Center (Heasarc) 2014)

APPENDIX

A. THE CATALOG

This appendix presents all bursts identified in this study. Magnetars for which at least one burst was detected include CXOU J010043.1–721134 (Table 5), 4U 0142+61 (Table 6), 1E 1048.1–5937 (Table 7), Swift J1555.2–5402 (Table 8), 1RXS J170849.0–400910 (Table 9), SGR 1806–20 (Table 10), XTE J1810–197 (Table 11), Swift J1818.0–1607 (Table 12), Swift J1822.3–1606 (Table 13), SGR 1830–0645 (Table 14), 1E 1841–045 (Table 15), SGR 1935+2154 (Table 16), 1E 2259+586 (Table 17), and the magnetar-like pulsar PSR J1846–0258 (Table 18). For magnetars with more than 30 detected bursts, a complete burst catalog is provided as an online table.

Table 5. Burst catalog of magnetar CXOU J010043.1–721134

Burst	ObsID	TDB start	T_{90} (ms)	HR	kT^* (keV)	F_{BB} (erg cm $^{-2}$ s $^{-1}$)	Γ	F_{PL} (erg cm $^{-2}$ s $^{-1}$)
1	5505010502	2022-07-24T23:59:07.273	0.005	-0.87 ± 0.09	$0.40^{+0.07}_{-0.05}$	$-5.06^{+0.08}_{-0.08}$	$2.50^{+0.38}_{-0.37}$	$-4.93^{+0.09}_{-0.09}$
2	5505011602	2023-06-24T12:28:23.950	795.595	0.04 ± 0.14	—	$-8.63^{+0.09}_{-0.13}$	$-0.92^{+0.28}_{-0.29}$	$-8.62^{+0.10}_{-0.10}$
3	5505011703	2023-07-30T22:40:23.300	250.465	-0.64 ± 0.16	1.2	$-9.27^{+0.09}_{-0.10}$	0.8	$-9.14^{+0.09}_{-0.10}$
4	5505011704	2023-07-31T20:21:10.490	1055.592	-0.74 ± 0.07	$1.36^{+0.19}_{-0.15}$	$-9.36^{+0.09}_{-0.08}$	$0.36^{+0.18}_{-0.18}$	$-9.14^{+0.08}_{-0.08}$

* Burst for which kT could not be constrained during spectral fitting is marked with “—”

Table 6. Burst catalog of magnetar 4U 0142+61

Burst	ObsID	TDB start	T_{90} (ms)	HR	kT (keV)	F_{BB} (erg cm $^{-2}$ s $^{-1}$)	Γ	F_{PL} (erg cm $^{-2}$ s $^{-1}$)
1	0020040102	2017-07-15T14:15:37.947	27.684	-0.56 ± 0.16	$0.96^{+0.22}_{-0.16}$	$-8.28^{+0.12}_{-0.11}$	$1.32^{+0.39}_{-0.38}$	$-8.14^{+0.12}_{-0.11}$
2	2598061601	2019-10-20T00:30:01.984	10.171	-1.00 ± 0.02	1.2	$-8.12^{+0.13}_{-0.14}$	0.8	$-7.95^{+0.13}_{-0.14}$
3	4549061701	2021-10-22T01:41:59.761	19.641	-1.00 ± 0.01	1.2	$-8.35^{+0.12}_{-0.13}$	0.8	$-8.18^{+0.12}_{-0.13}$
4	6020040102	2023-09-26T11:56:38.889	287.419	-0.86 ± 0.08	$0.48^{+0.07}_{-0.05}$	$-9.15^{+0.07}_{-0.07}$	$2.55^{+0.36}_{-0.34}$	$-8.94^{+0.07}_{-0.07}$

Table 7. Burst catalog of magnetar 1E 1048.1–5937

Burst	ObsID	TDB start	T_{90} (ms)	HR	kT (keV)	F_{BB} (erg cm $^{-2}$ s $^{-1}$)	Γ	F_{PL} (erg cm $^{-2}$ s $^{-1}$)
1	1020240141	2018-11-22T11:58:14.425	0.001	-0.71 ± 0.26	1.2	$-4.55^{+0.15}_{-0.17}$	0.8	$-4.38^{+0.15}_{-0.17}$

Table 8. Burst catalog of magnetar Swift J1555.2–5402

Burst	ObsID	TDB start	T_{90} (ms)	HR	kT (keV)	F_{BB} (erg cm $^{-2}$ s $^{-1}$)	Γ	F_{PL} (erg cm $^{-2}$ s $^{-1}$)
1	4202190101	2021-06-03T13:58:12.407	15.382	-0.27 ± 0.29	1.2	$-7.85^{+0.12}_{-0.14}$	0.8	$-7.67^{+0.12}_{-0.14}$
2	4202190101	2021-06-03T13:58:30.247	68.397	0.09 ± 0.30	1.2	$-8.49^{+0.12}_{-0.14}$	0.8	$-8.31^{+0.12}_{-0.14}$
3	4202190101	2021-06-03T14:01:43.339	18.493	0.31 ± 0.19	$2.57^{+2.58}_{-0.80}$	$-7.43^{+0.15}_{-0.13}$	$0.04^{+0.60}_{-0.62}$	$-7.35^{+0.12}_{-0.11}$
4	4202190101	2021-06-03T14:08:53.301	13.170	0.50 ± 0.31	1.2	$-7.92^{+0.14}_{-0.16}$	0.8	$-7.74^{+0.14}_{-0.16}$
5	4202190101	2021-06-03T18:56:09.216	3.999	0.00 ± 0.41	1.2	$-7.53^{+0.17}_{-0.19}$	0.8	$-7.34^{+0.17}_{-0.19}$
6	4560010101	2021-06-04T14:44:33.324	14.713	0.25 ± 0.34	1.2	$-7.97^{+0.14}_{-0.16}$	0.8	$-7.79^{+0.14}_{-0.16}$
7	4560010101	2021-06-04T14:50:53.414	15.933	0.53 ± 0.21	1.2	$-7.68^{+0.10}_{-0.11}$	0.8	$-7.49^{+0.10}_{-0.11}$
8	4560010102	2021-06-05T14:02:44.083	16.026	0.71 ± 0.26	1.2	$-8.06^{+0.15}_{-0.17}$	0.8	$-7.88^{+0.15}_{-0.17}$
9	4560010102	2021-06-05T15:49:04.054	15.114	0.33 ± 0.31	1.2	$-7.93^{+0.14}_{-0.15}$	0.8	$-7.75^{+0.14}_{-0.15}$
10	4560010102	2021-06-05T15:50:02.211	15.034	0.75 ± 0.23	1.2	$-7.98^{+0.14}_{-0.16}$	0.8	$-7.79^{+0.14}_{-0.16}$
11	4560010102	2021-06-05T17:18:34.725	6.273	0.67 ± 0.30	1.2	$-7.72^{+0.17}_{-0.19}$	0.8	$-7.54^{+0.17}_{-0.19}$
12	4560010102	2021-06-05T17:19:28.827	1.912	0.20 ± 0.44	1.2	$-7.29^{+0.18}_{-0.21}$	0.8	$-7.10^{+0.18}_{-0.21}$
13	4560010102	2021-06-05T22:02:08.210	96.565	-0.08 ± 0.28	1.2	$-8.57^{+0.12}_{-0.13}$	0.8	$-8.39^{+0.12}_{-0.13}$
14	4560010102	2021-06-05T23:38:47.741	11.873	0.25 ± 0.34	1.2	$-7.87^{+0.14}_{-0.16}$	0.8	$-7.69^{+0.14}_{-0.16}$
15	4560010105	2021-06-08T00:37:11.129	21.066	0.67 ± 0.30	1.2	$-8.25^{+0.17}_{-0.19}$	0.8	$-8.07^{+0.17}_{-0.19}$
16	4560010105	2021-06-08T11:26:42.315	12.274	0.33 ± 0.31	1.2	$-7.84^{+0.14}_{-0.15}$	0.8	$-7.66^{+0.14}_{-0.15}$
17	4560010105	2021-06-08T11:30:17.135	3.891	0.00 ± 0.41	1.2	$-7.52^{+0.17}_{-0.19}$	0.8	$-7.33^{+0.17}_{-0.19}$
18	4560010201	2021-06-09T05:58:17.772	20.052	0.33 ± 0.22	1.2	$-7.74^{+0.10}_{-0.11}$	0.8	$-7.56^{+0.10}_{-0.11}$
19	4560010201	2021-06-09T07:31:09.537	10.284	0.43 ± 0.34	1.2	$-7.86^{+0.15}_{-0.17}$	0.8	$-7.68^{+0.15}_{-0.17}$
20	4560010201	2021-06-09T10:41:20.317	8.136	0.14 ± 0.37	1.2	$-7.77^{+0.15}_{-0.17}$	0.8	$-7.59^{+0.15}_{-0.17}$
21	4560010201	2021-06-09T13:48:15.408	21.464	0.08 ± 0.28	1.2	$-7.92^{+0.12}_{-0.13}$	0.8	$-7.74^{+0.12}_{-0.13}$
22	4560010201	2021-06-09T13:49:47.011	20.901	0.50 ± 0.31	1.2	$-8.12^{+0.14}_{-0.16}$	0.8	$-7.94^{+0.14}_{-0.16}$
23	4560010202	2021-06-10T02:07:01.017	14.500	0.75 ± 0.23	1.2	$-7.96^{+0.14}_{-0.16}$	0.8	$-7.78^{+0.14}_{-0.16}$
24	4560010202	2021-06-10T05:12:16.355	25.015	-0.11 ± 0.33	1.2	$-8.14^{+0.14}_{-0.15}$	0.8	$-7.96^{+0.14}_{-0.15}$
25	4560010301	2021-06-11T10:46:48.341	7.549	0.33 ± 0.38	1.2	$-7.80^{+0.17}_{-0.19}$	0.8	$-7.62^{+0.17}_{-0.19}$
26	4560010602	2021-06-17T02:58:45.587	4.830	-0.04 ± 0.20	$2.63^{+2.91}_{-0.85}$	$-6.82^{+0.15}_{-0.14}$	$0.22^{+0.61}_{-0.63}$	$-6.77^{+0.12}_{-0.11}$
27	4560010602	2021-06-17T03:00:05.180	44.434	0.43 ± 0.12	$3.12^{+2.37}_{-0.88}$	$-7.50^{+0.11}_{-0.10}$	$-0.13^{+0.42}_{-0.43}$	$-7.44^{+0.09}_{-0.08}$
28	4560010602	2021-06-17T03:06:05.556	30.304	0.11 ± 0.33	1.2	$-8.23^{+0.14}_{-0.15}$	0.8	$-8.05^{+0.14}_{-0.15}$
29	4560010701	2021-06-19T04:34:47.771	24.491	0.14 ± 0.37	1.2	$-8.25^{+0.15}_{-0.17}$	0.8	$-8.06^{+0.15}_{-0.17}$
30	4560010701	2021-06-19T04:39:46.659	7.865	0.25 ± 0.34	1.2	$-7.70^{+0.14}_{-0.16}$	0.8	$-7.51^{+0.14}_{-0.16}$
...
74	4560013017	2021-10-23T06:18:22.667	22.435	-0.33 ± 0.31	1.2	$-8.00^{+0.14}_{-0.15}$	0.8	$-7.82^{+0.14}_{-0.15}$

Table 9. Burst catalog of magnetar 1RXS J170849.0–400910

Burst	ObsID	TDB start	T_{90} (ms)	HR	kT^* (keV)	F_{BB} (erg cm $^{-2}$ s $^{-1}$)	Γ	F_{PL} (erg cm $^{-2}$ s $^{-1}$)
1	3622050401	2020-04-03T18:13:10.886	111.437	0.34 ± 0.09	—	$-7.70^{+0.04}_{-0.06}$	$-0.84^{+0.23}_{-0.24}$	$-7.74^{+0.07}_{-0.07}$

* Burst for which kT could not be constrained during spectral fitting is marked with “—”

Table 10. Burst catalog of magnetar SGR 1806–20

Burst	ObsID	TDB start	T_{90} (ms)	HR	kT (keV)	F_{BB} (erg cm $^{-2}$ s $^{-1}$)	Γ	F_{PL} (erg cm $^{-2}$ s $^{-1}$)
1	5020410102	2023-02-25T00:23:44.944	136.532	0.37 ± 0.04	$2.14^{+0.19}_{-0.16}$	$-7.00^{+0.03}_{-0.02}$	$0.45^{+0.14}_{-0.14}$	$-6.92^{+0.02}_{-0.02}$
2	5020410102	2023-02-25T00:33:59.721	171.007	0.56 ± 0.10	$3.78^{+3.97}_{-1.18}$	$-7.91^{+0.09}_{-0.09}$	$-0.20^{+0.42}_{-0.43}$	$-7.88^{+0.07}_{-0.07}$
3	5020410102	2023-02-25T01:32:03.158	163.288	0.33 ± 0.16	$1.30^{+0.32}_{-0.21}$	$-8.21^{+0.07}_{-0.08}$	$1.38^{+0.54}_{-0.55}$	$-8.03^{+0.10}_{-0.08}$
4	5020410103	2023-02-28T21:10:53.593	355.533	0.47 ± 0.02	$3.20^{+0.23}_{-0.20}$	$-6.50^{+0.01}_{-0.01}$	$-0.06^{+0.07}_{-0.07}$	$-6.45^{+0.01}_{-0.01}$

Table 11. Burst catalog of magnetar XTE J1810–197

Burst	ObsID	TDB start	T_{90} (ms)	HR	kT^* (keV)	F_{BB} (erg cm $^{-2}$ s $^{-1}$)	Γ	F_{PL} (erg cm $^{-2}$ s $^{-1}$)
1	2020420105	2019-03-31T22:57:55.917	195.301	0.38 ± 0.10	—	$-7.81^{+0.04}_{-0.05}$	$-1.40^{+0.25}_{-0.26}$	$-7.75^{+0.07}_{-0.08}$

* Burst for which kT could not be constrained during spectral fitting is marked with “—”

Table 12. Burst catalog of magnetar Swift J1818.0–1607

Burst	ObsID	TDB start	T_{90} (ms)	HR	kT^* (keV)	F_{BB} (erg cm $^{-2}$ s $^{-1}$)	Γ	F_{PL} (erg cm $^{-2}$ s $^{-1}$)
1	3201060101	2020-03-13T04:47:22.249	17.981	0.80 ± 0.19	1.2	$-7.85^{+0.13}_{-0.14}$	0.8	$-7.67^{+0.13}_{-0.14}$
2	3201060101	2020-03-13T06:06:49.313	94.302	0.64 ± 0.23	1.2	$-8.53^{+0.12}_{-0.14}$	0.8	$-8.36^{+0.12}_{-0.14}$
3	3556010301	2020-03-19T18:42:30.401	32.664	0.36 ± 0.20	$2.34^{+2.38}_{-0.73}$	$-7.69^{+0.15}_{-0.13}$	$0.35^{+0.69}_{-0.71}$	$-7.62^{+0.12}_{-0.11}$
4	3556010401	2020-03-20T11:40:17.451	17.572	0.50 ± 0.31	1.2	$-7.93^{+0.14}_{-0.16}$	0.8	$-7.76^{+0.14}_{-0.16}$
5	3556010401	2020-03-20T19:25:38.571	13.051	-0.60 ± 0.36	1.2	$-8.02^{+0.18}_{-0.21}$	0.8	$-7.84^{+0.18}_{-0.21}$
6	3556010501	2020-03-21T01:43:57.860	16.816	0.33 ± 0.24	1.2	$-7.67^{+0.11}_{-0.12}$	0.8	$-7.49^{+0.11}_{-0.12}$
7	3556010501	2020-03-21T09:02:31.782	11.639	0.20 ± 0.31	1.2	$-7.68^{+0.13}_{-0.14}$	0.8	$-7.51^{+0.13}_{-0.14}$
8	3556011501	2020-03-30T08:40:42.423	4.766	0.33 ± 0.22	1.2	$-7.04^{+0.10}_{-0.11}$	0.8	$-6.87^{+0.10}_{-0.11}$
9	3556011502	2020-03-31T12:37:33.925	16.717	0.37 ± 0.21	1.2	$-7.56^{+0.10}_{-0.10}$	0.8	$-7.39^{+0.10}_{-0.10}$
10	3556011502	2020-03-31T12:45:41.940	7.767	0.54 ± 0.23	1.2	$-7.40^{+0.12}_{-0.13}$	0.8	$-7.22^{+0.12}_{-0.13}$
11	3556011601	2020-04-03T13:20:28.393	4.307	0.43 ± 0.34	1.2	$-7.40^{+0.15}_{-0.17}$	0.8	$-7.22^{+0.15}_{-0.17}$
12	3556011801	2020-04-08T05:25:28.223	1.836	0.67 ± 0.30	1.2	$-7.10^{+0.17}_{-0.19}$	0.8	$-6.92^{+0.17}_{-0.19}$
13	3556012001	2020-04-14T21:06:03.679	49.414	0.27 ± 0.29	1.2	$-8.27^{+0.12}_{-0.14}$	0.8	$-8.10^{+0.12}_{-0.14}$
14	3556012301	2020-04-23T07:51:42.142	17.795	0.69 ± 0.20	1.2	$-7.76^{+0.12}_{-0.13}$	0.8	$-7.59^{+0.12}_{-0.13}$
15	3556012401	2020-04-27T08:01:52.434	22.607	0.36 ± 0.20	—	$-7.41^{+0.12}_{-0.16}$	$-0.66^{+0.74}_{-0.77}$	$-7.42^{+0.15}_{-0.14}$
16	3556012501	2020-04-29T22:01:37.866	64.451	0.41 ± 0.18	$3.19^{+6.53}_{-1.16}$	$-7.84^{+0.15}_{-0.13}$	$-0.13^{+0.63}_{-0.65}$	$-7.79^{+0.12}_{-0.11}$
17	3556012602	2020-05-03T06:16:44.138	16.749	-0.25 ± 0.34	1.2	$-7.95^{+0.14}_{-0.16}$	0.8	$-7.77^{+0.14}_{-0.16}$
18	3556012602	2020-05-03T07:51:32.437	46.881	0.14 ± 0.26	1.2	$-8.15^{+0.11}_{-0.12}$	0.8	$-7.98^{+0.11}_{-0.12}$
19	3556012602	2020-05-03T18:35:55.093	5.422	0.60 ± 0.25	1.2	$-7.36^{+0.13}_{-0.14}$	0.8	$-7.19^{+0.13}_{-0.14}$
20	3556012701	2020-05-05T03:17:15.436	54.100	0.40 ± 0.29	1.2	$-8.36^{+0.13}_{-0.14}$	0.8	$-8.19^{+0.13}_{-0.14}$
21	3556012901	2020-05-20T23:01:47.068	49.164	-0.14 ± 0.37	1.2	$-8.47^{+0.15}_{-0.17}$	0.8	$-8.30^{+0.15}_{-0.17}$
22	3556013401	2020-06-05T00:00:36.972	3.188	0.33 ± 0.31	1.2	$-7.18^{+0.14}_{-0.15}$	0.8	$-7.00^{+0.14}_{-0.15}$
23	3556013701	2020-06-14T03:57:27.920	40.289	0.51 ± 0.10	$3.13^{+1.87}_{-0.80}$	$-7.57^{+0.09}_{-0.08}$	$-0.18^{+0.38}_{-0.39}$	$-7.50^{+0.07}_{-0.07}$
24	3556013901	2020-06-20T10:39:12.226	14.965	-0.33 ± 0.38	1.2	$-8.02^{+0.17}_{-0.19}$	0.8	$-7.85^{+0.17}_{-0.19}$
25	3556014302	2020-07-02T02:31:37.178	3.395	0.50 ± 0.43	1.2	$-7.56^{+0.20}_{-0.24}$	0.8	$-7.38^{+0.20}_{-0.24}$
26	3556014302	2020-07-02T05:35:54.337	28.858	0.17 ± 0.28	1.2	$-8.01^{+0.12}_{-0.13}$	0.8	$-7.83^{+0.12}_{-0.13}$
27	3556015201	2020-08-25T09:48:03.712	53.695	0.46 ± 0.27	1.2	$-8.30^{+0.12}_{-0.14}$	0.8	$-8.13^{+0.12}_{-0.14}$

* Burst for which kT could not be constrained during spectral fitting is marked with “—”

Table 13. Burst catalog of magnetar Swift J1822.3–1606

Burst	ObsID	TDB start	T_{90} (ms)	HR	kT^* (keV)	F_{BB} (erg cm $^{-2}$ s $^{-1}$)	Γ	F_{PL} (erg cm $^{-2}$ s $^{-1}$)
1	1020460110	2018-04-11T19:53:02.682	206.345	0.21 ± 0.17	—	$-8.43^{+0.13}_{-0.16}$	$-0.76^{+0.36}_{-0.38}$	$-8.43^{+0.12}_{-0.13}$

* Burst for which kT could not be constrained during spectral fitting is marked with “—”

Table 14. Burst catalog of magnetar SGR 1830–0645

Burst	ObsID	TDB start	T_{90} (ms)	HR	kT (keV)	F_{BB} (erg cm $^{-2}$ s $^{-1}$)	Γ	F_{PL} (erg cm $^{-2}$ s $^{-1}$)
1	3201810102	2020-10-11T13:13:22.627	14.583	-0.14 ± 0.37	1.2	$-8.42^{+0.15}_{-0.17}$	0.8	$-8.25^{+0.15}_{-0.17}$
2	3201810103	2020-10-12T03:08:29.432	23.174	-0.16 ± 0.23	1.2	$-8.18^{+0.10}_{-0.10}$	0.8	$-8.01^{+0.10}_{-0.10}$
3	3201810103	2020-10-12T11:06:46.629	15.462	-0.50 ± 0.31	1.2	$-8.37^{+0.14}_{-0.16}$	0.8	$-8.20^{+0.14}_{-0.16}$
4	3201810104	2020-10-13T02:24:26.198	11.321	-0.71 ± 0.26	1.2	$-8.31^{+0.15}_{-0.17}$	0.8	$-8.14^{+0.15}_{-0.17}$
5	3201810104	2020-10-13T02:25:43.723	27.985	-0.78 ± 0.21	1.2	$-8.60^{+0.14}_{-0.15}$	0.8	$-8.42^{+0.14}_{-0.15}$
6	3201810104	2020-10-13T04:12:47.104	43.532	-0.48 ± 0.18	$1.21^{+0.36}_{-0.23}$	$-8.44^{+0.15}_{-0.13}$	$0.75^{+0.42}_{-0.42}$	$-8.26^{+0.14}_{-0.14}$
7	3201810104	2020-10-13T08:51:13.440	31.461	-0.69 ± 0.20	1.2	$-8.49^{+0.12}_{-0.13}$	0.8	$-8.31^{+0.12}_{-0.13}$
8	3201810105	2020-10-14T05:53:25.046	17.298	-0.22 ± 0.23	1.2	$-8.05^{+0.10}_{-0.11}$	0.8	$-7.87^{+0.10}_{-0.11}$
9	3201810106	2020-10-17T12:51:50.936	55.452	-0.74 ± 0.12	$0.97^{+0.19}_{-0.14}$	$-8.47^{+0.11}_{-0.10}$	$1.09^{+0.36}_{-0.36}$	$-8.27^{+0.12}_{-0.11}$
10	3201810106	2020-10-17T13:02:25.535	18.565	-0.75 ± 0.23	1.2	$-8.42^{+0.14}_{-0.16}$	0.8	$-8.25^{+0.14}_{-0.16}$
11	3201810106	2020-10-17T17:32:44.182	44.246	-0.87 ± 0.13	1.2	$-8.53^{+0.11}_{-0.12}$	0.8	$-8.35^{+0.11}_{-0.12}$
12	3201810106	2020-10-17T19:03:51.189	11.280	-0.14 ± 0.37	1.2	$-8.26^{+0.15}_{-0.17}$	0.8	$-8.09^{+0.15}_{-0.17}$
13	3201810106	2020-10-17T19:05:45.315	6.752	-0.33 ± 0.31	1.2	$-7.93^{+0.14}_{-0.15}$	0.8	$-7.76^{+0.14}_{-0.15}$
14	3201810106	2020-10-17T20:39:40.869	6.332	0.25 ± 0.34	1.2	$-7.95^{+0.14}_{-0.16}$	0.8	$-7.78^{+0.14}_{-0.16}$
15	3201810106	2020-10-17T20:40:22.716	21.392	-0.82 ± 0.17	1.2	$-8.35^{+0.12}_{-0.14}$	0.8	$-8.17^{+0.12}_{-0.14}$
16	3201810106	2020-10-17T20:44:10.104	33.586	-0.32 ± 0.12	$1.65^{+0.35}_{-0.24}$	$-7.77^{+0.10}_{-0.09}$	$0.22^{+0.25}_{-0.25}$	$-7.60^{+0.09}_{-0.09}$
17	3201810106	2020-10-17T20:44:43.164	28.339	-0.23 ± 0.27	1.2	$-8.39^{+0.12}_{-0.13}$	0.8	$-8.22^{+0.12}_{-0.13}$
18	3201810106	2020-10-17T20:47:13.721	59.941	0.20 ± 0.31	1.2	$-8.83^{+0.13}_{-0.14}$	0.8	$-8.66^{+0.13}_{-0.14}$
19	3201810106	2020-10-17T20:49:17.019	22.958	-0.54 ± 0.23	1.2	$-8.30^{+0.12}_{-0.13}$	0.8	$-8.13^{+0.12}_{-0.13}$
20	3201810107	2020-10-18T05:52:55.466	11.258	-0.11 ± 0.33	1.2	$-8.15^{+0.14}_{-0.15}$	0.8	$-7.98^{+0.14}_{-0.15}$
21	3201810107	2020-10-18T06:03:31.423	41.537	-0.67 ± 0.22	1.2	$-8.60^{+0.12}_{-0.13}$	0.8	$-8.42^{+0.12}_{-0.13}$
22	3201810107	2020-10-18T07:38:29.114	17.312	0.00 ± 0.29	1.2	$-8.22^{+0.12}_{-0.13}$	0.8	$-8.04^{+0.12}_{-0.13}$
23	3201810107	2020-10-18T07:40:44.267	24.162	-0.33 ± 0.24	1.2	$-8.26^{+0.11}_{-0.12}$	0.8	$-8.09^{+0.11}_{-0.12}$
24	3201810108	2020-10-19T03:44:59.635	17.771	-0.50 ± 0.31	1.2	$-8.40^{+0.14}_{-0.16}$	0.8	$-8.23^{+0.14}_{-0.16}$
25	3201810108	2020-10-19T06:47:05.411	4.292	-0.67 ± 0.30	1.2	$-7.91^{+0.17}_{-0.19}$	0.8	$-7.74^{+0.17}_{-0.19}$
26	3201810108	2020-10-19T09:46:53.410	4.465	-0.67 ± 0.30	1.2	$-7.93^{+0.17}_{-0.19}$	0.8	$-7.75^{+0.17}_{-0.19}$
27	3201810108	2020-10-19T09:56:39.345	27.231	-0.42 ± 0.19	$1.27^{+0.39}_{-0.25}$	$-8.13^{+0.15}_{-0.14}$	$0.75^{+0.41}_{-0.41}$	$-7.97^{+0.14}_{-0.14}$
28	3201810108	2020-10-19T15:58:57.143	27.155	-0.65 ± 0.18	1.2	$-8.26^{+0.10}_{-0.11}$	0.8	$-8.09^{+0.10}_{-0.11}$
29	3201810109	2020-10-20T23:05:23.906	55.510	-0.48 ± 0.18	$1.29^{+0.40}_{-0.25}$	$-8.49^{+0.15}_{-0.14}$	$0.58^{+0.42}_{-0.42}$	$-8.29^{+0.14}_{-0.14}$
30	3201810109	2020-10-20T23:08:31.159	49.872	-0.69 ± 0.20	1.2	$-8.64^{+0.12}_{-0.13}$	0.8	$-8.47^{+0.12}_{-0.13}$
...
128	4201810109	2021-03-22T05:28:50.886	28.740	-0.27 ± 0.29	1.2	$-8.49^{+0.12}_{-0.14}$	0.8	$-8.32^{+0.12}_{-0.14}$

Table 15. Burst catalog of magnetar 1E 1841–045

Burst	ObsID	TDB start	T_{90} (ms)	HR	kT (keV)	F_{BB} (erg cm $^{-2}$ s $^{-1}$)	Γ	F_{PL} (erg cm $^{-2}$ s $^{-1}$)
1	7020500115	2024-08-21T05:47:16.995	275.708	-0.30 ± 0.20	1.2	$-8.91^{+0.09}_{-0.09}$	0.8	$-8.72^{+0.09}_{-0.09}$
2	7020500115	2024-08-21T05:53:42.996	125.542	-0.62 ± 0.20	1.2	$-8.73^{+0.10}_{-0.11}$	0.8	$-8.54^{+0.10}_{-0.11}$
3	7020500115	2024-08-21T05:55:46.567	1563.466	-0.37 ± 0.06	$1.46^{+0.13}_{-0.11}$	$-8.65^{+0.04}_{-0.04}$	$0.76^{+0.14}_{-0.14}$	$-8.53^{+0.04}_{-0.04}$
4	7020500115	2024-08-21T07:24:50.450	778.175	-0.74 ± 0.10	$0.80^{+0.11}_{-0.09}$	$-9.32^{+0.07}_{-0.07}$	$1.76^{+0.33}_{-0.33}$	$-9.13^{+0.06}_{-0.07}$
5	7020500115	2024-08-21T07:34:23.033	933.788	-0.70 ± 0.09	$0.75^{+0.08}_{-0.07}$	$-9.34^{+0.05}_{-0.06}$	$1.97^{+0.28}_{-0.28}$	$-9.13^{+0.05}_{-0.05}$
6	7020500115	2024-08-21T07:38:19.847	73.198	-0.29 ± 0.26	1.2	$-8.71^{+0.11}_{-0.12}$	0.8	$-8.52^{+0.11}_{-0.12}$
7	7020500115	2024-08-21T07:38:52.599	134.445	-0.14 ± 0.10	$1.80^{+0.34}_{-0.24}$	$-8.20^{+0.08}_{-0.07}$	$0.29^{+0.23}_{-0.23}$	$-8.07^{+0.07}_{-0.07}$
8	7020500115	2024-08-21T10:41:11.236	392.833	-0.20 ± 0.04	$2.02^{+0.15}_{-0.13}$	$-7.77^{+0.03}_{-0.03}$	$0.18^{+0.09}_{-0.09}$	$-7.66^{+0.03}_{-0.03}$
9	7020500115	2024-08-21T10:44:00.142	369.713	-0.36 ± 0.10	$1.32^{+0.17}_{-0.14}$	$-8.60^{+0.07}_{-0.06}$	$0.83^{+0.23}_{-0.23}$	$-8.46^{+0.06}_{-0.06}$
10	7020500115	2024-08-21T10:44:00.976	195.195	-0.30 ± 0.20	1.2	$-8.92^{+0.09}_{-0.09}$	0.8	$-8.73^{+0.09}_{-0.09}$
11	7020500116	2024-08-22T08:18:31.181	200.954	-0.40 ± 0.12	$1.26^{+0.20}_{-0.15}$	$-8.55^{+0.08}_{-0.08}$	$0.97^{+0.28}_{-0.27}$	$-8.41^{+0.07}_{-0.07}$
12	7020500119	2024-08-25T00:05:16.059	42.214	-0.24 ± 0.16	$2.22^{+1.03}_{-0.52}$	$-7.92^{+0.13}_{-0.12}$	$0.16^{+0.37}_{-0.38}$	$-7.84^{+0.11}_{-0.11}$
13	7020500133	2024-09-25T16:42:06.956	80.832	-0.44 ± 0.21	1.2	$-8.64^{+0.10}_{-0.11}$	0.8	$-8.45^{+0.10}_{-0.11}$
14	7020500136	2024-09-28T19:00:50.111	20.617	-0.64 ± 0.23	1.2	$-8.26^{+0.12}_{-0.14}$	0.8	$-8.06^{+0.12}_{-0.14}$
15	7582010112	2024-11-09T19:06:31.623	82.960	-0.58 ± 0.19	1.2	$-8.62^{+0.10}_{-0.10}$	0.8	$-8.43^{+0.10}_{-0.10}$

Table 16. Burst catalog of magnetar SGR 1935+2154

Burst	ObsID	TDB start	T_{90} (ms)	HR	kT (keV)	F_{BB} (erg cm $^{-2}$ s $^{-1}$)	Γ	F_{PL} (erg cm $^{-2}$ s $^{-1}$)
1	3020560101	2020-04-28T00:42:04.992	200.675	-0.17 ± 0.15	$2.17^{+0.90}_{-0.48}$	$-8.65^{+0.13}_{-0.12}$	$0.17^{+0.35}_{-0.35}$	$-8.56^{+0.10}_{-0.10}$
2	3020560101	2020-04-28T00:42:07.375	308.612	-0.35 ± 0.16	$1.44^{+0.39}_{-0.25}$	$-8.93^{+0.12}_{-0.11}$	$0.65^{+0.38}_{-0.38}$	$-8.78^{+0.11}_{-0.10}$
3	3020560101	2020-04-28T00:42:09.715	89.207	-0.67 ± 0.22	1.2	$-8.87^{+0.12}_{-0.13}$	0.8	$-8.68^{+0.12}_{-0.13}$
4	3020560101	2020-04-28T00:42:15.538	422.493	0.04 ± 0.01	$3.81^{+0.14}_{-0.13}$	$-7.22^{+0.01}_{-0.01}$	$-0.41^{+0.02}_{-0.02}$	$-7.15^{+0.01}_{-0.01}$
5	3020560101	2020-04-28T00:42:32.978	641.929	-0.20 ± 0.11	$1.69^{+0.32}_{-0.23}$	$-8.84^{+0.08}_{-0.08}$	$0.48^{+0.24}_{-0.25}$	$-8.72^{+0.07}_{-0.07}$
6	3020560101	2020-04-28T00:42:37.112	58.988	-0.60 ± 0.21	1.2	$-8.60^{+0.11}_{-0.12}$	0.8	$-8.41^{+0.11}_{-0.12}$
7	3020560101	2020-04-28T00:42:40.065	1452.321	-0.32 ± 0.07	$1.50^{+0.15}_{-0.13}$	$-8.83^{+0.05}_{-0.05}$	$0.58^{+0.16}_{-0.16}$	$-8.69^{+0.05}_{-0.04}$
8	3020560101	2020-04-28T00:42:43.945	97.369	-0.17 ± 0.18	$1.66^{+0.60}_{-0.35}$	$-8.44^{+0.14}_{-0.13}$	$0.72^{+0.41}_{-0.42}$	$-8.36^{+0.12}_{-0.11}$
9	3020560101	2020-04-28T00:42:44.229	48.001	-0.43 ± 0.24	1.2	$-8.54^{+0.11}_{-0.12}$	0.8	$-8.35^{+0.11}_{-0.12}$
10	3020560101	2020-04-28T00:42:45.235	569.746	-0.13 ± 0.03	$2.14^{+0.14}_{-0.12}$	$-7.88^{+0.03}_{-0.03}$	$0.05^{+0.08}_{-0.08}$	$-7.76^{+0.02}_{-0.02}$
11	3020560101	2020-04-28T00:42:52.979	166.817	-0.78 ± 0.15	1.2	$-8.96^{+0.10}_{-0.11}$	0.8	$-8.77^{+0.10}_{-0.11}$
12	3020560101	2020-04-28T00:42:57.998	472.229	-0.51 ± 0.08	$1.32^{+0.15}_{-0.12}$	$-8.65^{+0.06}_{-0.06}$	$0.74^{+0.20}_{-0.20}$	$-8.49^{+0.06}_{-0.05}$
13	3020560101	2020-04-28T00:43:05.677	25.986	-0.27 ± 0.29	1.2	$-8.38^{+0.12}_{-0.14}$	0.8	$-8.19^{+0.12}_{-0.14}$
14	3020560101	2020-04-28T00:43:10.501	509.074	-0.35 ± 0.10	$1.31^{+0.18}_{-0.14}$	$-8.78^{+0.07}_{-0.07}$	$0.84^{+0.24}_{-0.24}$	$-8.63^{+0.07}_{-0.06}$
15	3020560101	2020-04-28T00:43:27.446	222.850	-0.25 ± 0.11	$1.91^{+0.43}_{-0.29}$	$-8.44^{+0.09}_{-0.08}$	$0.19^{+0.25}_{-0.25}$	$-8.31^{+0.08}_{-0.07}$
16	3020560101	2020-04-28T00:43:29.533	234.156	-0.29 ± 0.23	1.2	$-9.14^{+0.10}_{-0.11}$	0.8	$-8.95^{+0.10}_{-0.11}$
17	3020560101	2020-04-28T00:43:31.919	327.903	-0.49 ± 0.14	$0.95^{+0.16}_{-0.12}$	$-9.04^{+0.08}_{-0.08}$	$1.44^{+0.36}_{-0.36}$	$-8.86^{+0.08}_{-0.08}$
18	3020560101	2020-04-28T00:43:35.627	998.136	-0.18 ± 0.03	$1.98^{+0.09}_{-0.08}$	$-7.93^{+0.02}_{-0.02}$	$0.16^{+0.06}_{-0.06}$	$-7.80^{+0.02}_{-0.02}$
19	3020560101	2020-04-28T00:43:38.163	355.770	-0.07 ± 0.03	$2.57^{+0.19}_{-0.17}$	$-7.86^{+0.03}_{-0.03}$	$-0.12^{+0.07}_{-0.07}$	$-7.77^{+0.02}_{-0.02}$
20	3020560101	2020-04-28T00:43:45.520	955.644	-0.10 ± 0.09	$2.06^{+0.39}_{-0.28}$	$-8.78^{+0.07}_{-0.07}$	$0.10^{+0.21}_{-0.21}$	$-8.65^{+0.06}_{-0.06}$
21	3020560101	2020-04-28T00:43:52.985	1904.002	-0.32 ± 0.05	$1.59^{+0.13}_{-0.11}$	$-8.74^{+0.04}_{-0.04}$	$0.47^{+0.12}_{-0.12}$	$-8.60^{+0.04}_{-0.04}$
22	3020560101	2020-04-28T00:44:00.547	445.025	-0.62 ± 0.13	$1.03^{+0.19}_{-0.14}$	$-9.17^{+0.09}_{-0.09}$	$1.15^{+0.36}_{-0.36}$	$-8.98^{+0.09}_{-0.09}$
23	3020560101	2020-04-28T00:44:06.233	235.896	-0.21 ± 0.06	$1.87^{+0.20}_{-0.16}$	$-7.89^{+0.05}_{-0.05}$	$0.25^{+0.14}_{-0.14}$	$-7.77^{+0.04}_{-0.04}$
24	3020560101	2020-04-28T00:44:07.030	183.750	-0.22 ± 0.12	$1.61^{+0.31}_{-0.22}$	$-8.49^{+0.09}_{-0.08}$	$0.47^{+0.26}_{-0.26}$	$-8.36^{+0.08}_{-0.08}$
25	3020560101	2020-04-28T00:44:07.493	334.338	-0.37 ± 0.12	$1.61^{+0.34}_{-0.24}$	$-8.69^{+0.09}_{-0.09}$	$0.45^{+0.28}_{-0.28}$	$-8.55^{+0.08}_{-0.08}$
26	3020560101	2020-04-28T00:44:08.441	735.361	-0.03 ± 0.01	$2.99^{+0.08}_{-0.08}$	$-6.99^{+0.01}_{-0.01}$	$-0.25^{+0.02}_{-0.02}$	$-6.91^{+0.01}_{-0.01}$
27	3020560101	2020-04-28T00:44:10.635	120.500	-0.02 ± 0.10	$4.28^{+2.82}_{-1.15}$	$-7.77^{+0.08}_{-0.08}$	$-0.43^{+0.23}_{-0.23}$	$-7.73^{+0.07}_{-0.07}$
28	3020560101	2020-04-28T00:44:17.045	901.641	-0.49 ± 0.09	$1.18^{+0.15}_{-0.12}$	$-9.07^{+0.06}_{-0.06}$	$0.95^{+0.23}_{-0.23}$	$-8.90^{+0.06}_{-0.06}$
29	3020560101	2020-04-28T00:44:19.704	425.656	-0.26 ± 0.09	$1.59^{+0.23}_{-0.18}$	$-8.56^{+0.07}_{-0.06}$	$0.48^{+0.21}_{-0.21}$	$-8.42^{+0.06}_{-0.06}$
30	3020560101	2020-04-28T00:44:20.470	56.817	-0.11 ± 0.14	$2.00^{+0.66}_{-0.39}$	$-8.00^{+0.11}_{-0.11}$	$0.24^{+0.32}_{-0.33}$	$-7.90^{+0.10}_{-0.10}$
...
867	5576010116	2022-11-15T11:48:59.834	222.401	-0.37 ± 0.21	1.2	$-8.97^{+0.10}_{-0.10}$	0.8	$-8.78^{+0.10}_{-0.10}$

Table 17. Burst catalog of magnetar 1E 2259+586

Burst	ObsID	TDB start	T_{90} (ms)	HR	kT (keV)	F_{BB} (erg cm $^{-2}$ s $^{-1}$)	Γ	F_{PL} (erg cm $^{-2}$ s $^{-1}$)
1	7020600108	2024-12-27T21:14:02.224	236.260	-1.00 ± 0.00	1.2	$-9.15^{+0.09}_{-0.10}$	0.8	$-8.98^{+0.09}_{-0.10}$

Table 18. Burst catalog of magnetar PSR J1846–0258

Burst	ObsID	TDB start	T_{90} (ms)	HR	kT (keV)	F_{BB} (erg cm $^{-2}$ s $^{-1}$)	Γ	F_{PL} (erg cm $^{-2}$ s $^{-1}$)
1	3033290103	2020-08-05T17:08:55.807	20.480	0.12 ± 0.25	1.2	$-7.91^{+0.10}_{-0.11}$	0.8	$-7.72^{+0.10}_{-0.11}$
2	3033290104	2020-08-06T22:25:26.265	32.558	-0.31 ± 0.19	$1.33^{+0.40}_{-0.25}$	$-7.99^{+0.11}_{-0.10}$	$0.97^{+0.52}_{-0.53}$	$-7.84^{+0.10}_{-0.09}$
3	3033290108	2020-08-10T08:51:46.075	10.516	-0.71 ± 0.26	1.2	$-7.97^{+0.15}_{-0.17}$	0.8	$-7.78^{+0.15}_{-0.17}$
4	3598010801	2020-07-25T19:38:03.338	11.285	0.25 ± 0.34	1.2	$-7.95^{+0.14}_{-0.16}$	0.8	$-7.76^{+0.14}_{-0.16}$

REFERENCES

- Archibald, R. F., Kaspi, V. M., Tendulkar, S. P., & Scholz, P. 2016, ApJL, 829, L21, doi: [10.3847/2041-8205/829/1/L21](https://doi.org/10.3847/2041-8205/829/1/L21)
- Bochenek, C. D., Ravi, V., Belov, K. V., et al. 2020, Nature, 587, 59, doi: [10.1038/s41586-020-2872-x](https://doi.org/10.1038/s41586-020-2872-x)
- Borghese, A., Rea, N., Turolla, R., et al. 2021, MNRAS, 504, 5244, doi: [10.1093/mnras/stab1236](https://doi.org/10.1093/mnras/stab1236)
- CHIME/FRB Collaboration, Andersen, B. C., Bandura, K. M., et al. 2020, Nature, 587, 54, doi: [10.1038/s41586-020-2863-y](https://doi.org/10.1038/s41586-020-2863-y)
- Chu, C.-Y., & Chang, H.-K. 2023, MNRAS, 526, 1287, doi: [10.1093/mnras/stad2874](https://doi.org/10.1093/mnras/stad2874)
- Collazzi, A. C., Kouveliotou, C., van der Horst, A. J., et al. 2015, ApJS, 218, 11, doi: [10.1088/0067-0049/218/1/11](https://doi.org/10.1088/0067-0049/218/1/11)
- Coti Zelati, F., Rea, N., Pons, J. A., Campana, S., & Esposito, P. 2018, MNRAS, 474, 961, doi: [10.1093/mnras/stx2679](https://doi.org/10.1093/mnras/stx2679)
- Dong, F. A., & Chime/FRB Collaboration. 2022, The Astronomer's Telegram, 15681, 1
- Duncan, R. C., & Thompson, C. 1992, ApJL, 392, L9, doi: [10.1086/186413](https://doi.org/10.1086/186413)
- Enoto, T., Ng, M., Hu, C.-P., et al. 2021, ApJL, 920, L4, doi: [10.3847/2041-8213/ac2665](https://doi.org/10.3847/2041-8213/ac2665)
- Gavriil, F. P., Gonzalez, M. E., Gotthelf, E. V., et al. 2008, Science, 319, 1802, doi: [10.1126/science.1153465](https://doi.org/10.1126/science.1153465)
- Gavriil, F. P., Kaspi, V. M., & Woods, P. M. 2002, Nature, 419, 142, doi: [10.1038/nature01011](https://doi.org/10.1038/nature01011)
- Gendreau, K. C., Arzoumanian, Z., Adkins, P. W., et al. 2016, in Society of Photo-Optical Instrumentation Engineers (SPIE) Conference Series, Vol. 9905, Space Telescopes and Instrumentation 2016: Ultraviolet to Gamma Ray, ed. J.-W. A. den Herder, T. Takahashi, & M. Bautz, 99051H, doi: [10.1117/12.2231304](https://doi.org/10.1117/12.2231304)
- Giri, U., Andersen, B. C., Chawla, P., et al. 2023, arXiv e-prints, arXiv:2310.16932, doi: [10.48550/arXiv.2310.16932](https://doi.org/10.48550/arXiv.2310.16932)
- Gotthelf, E. V., Halpern, J. P., Alford, J. A. J., et al. 2019, ApJL, 874, L25, doi: [10.3847/2041-8213/ab101a](https://doi.org/10.3847/2041-8213/ab101a)
- Göğüş, E., Lin, L., Kaneko, Y., et al. 2016, ApJL, 829, L25, doi: [10.3847/2041-8205/829/2/L25](https://doi.org/10.3847/2041-8205/829/2/L25)
- Göğüş, E., Kouveliotou, C., Woods, P. M., et al. 2001, ApJ, 558, 228, doi: [10.1086/322463](https://doi.org/10.1086/322463)
- Guver, T., Hu, C.-P., Younes, G., et al. 2021, The Astronomer's Telegram, 14916, 1
- Guver, T., Göğüş, E., Vurgun, E., et al. 2019, ApJL, 877, L30, doi: [10.3847/2041-8213/ab212d](https://doi.org/10.3847/2041-8213/ab212d)
- Hu, C.-P., Begiçarslan, B., Güver, T., et al. 2020, ApJ, 902, 1, doi: [10.3847/1538-4357/abb3c9](https://doi.org/10.3847/1538-4357/abb3c9)
- Hu, C.-P., Kuiper, L., Harding, A. K., et al. 2023, ApJ, 952, 120, doi: [10.3847/1538-4357/acd850](https://doi.org/10.3847/1538-4357/acd850)
- Hu, C.-P., Wadiasingh, Z., Ho, W. C. G., et al. 2025, ApJ, 989, 63, doi: [10.3847/1538-4357/adea4e](https://doi.org/10.3847/1538-4357/adea4e)
- Jahoda, K., Markwardt, C. B., Radeva, Y., et al. 2006, ApJS, 163, 401, doi: [10.1086/500659](https://doi.org/10.1086/500659)
- Kırmızıbayrak, D., Şaşmaz Muş, S., Kaneko, Y., & Göğüş, E. 2017, ApJS, 232, 17, doi: [10.3847/1538-4365/aa88b7](https://doi.org/10.3847/1538-4365/aa88b7)
- Kirsten, F., Snelders, M. P., Jenkins, M., et al. 2021, Nature Astronomy, 5, 414, doi: [10.1038/s41550-020-01246-3](https://doi.org/10.1038/s41550-020-01246-3)
- Kouveliotou, C., Meegan, C. A., Fishman, G. J., et al. 1993, ApJL, 413, L101, doi: [10.1086/186969](https://doi.org/10.1086/186969)
- Li, C. K., Lin, L., Xiong, S. L., et al. 2021, Nature Astronomy, 5, 378, doi: [10.1038/s41550-021-01302-6](https://doi.org/10.1038/s41550-021-01302-6)
- Lin, L., Göğüş, E., Kaneko, Y., & Kouveliotou, C. 2013, ApJ, 778, 105, doi: [10.1088/0004-637X/778/2/105](https://doi.org/10.1088/0004-637X/778/2/105)
- Mazets, E. P., Golenetskij, S. V., & Guryan, Y. A. 1979a, Soviet Astronomy Letters, 5, 343
- Mazets, E. P., Golentskii, S. V., Ilinskii, V. N., Aptekar, R. L., & Guryan, I. A. 1979b, Nature, 282, 587, doi: [10.1038/282587a0](https://doi.org/10.1038/282587a0)
- Mereghetti, S., Savchenko, V., Ferrigno, C., et al. 2020, ApJL, 898, L29, doi: [10.3847/2041-8213/aba2cf](https://doi.org/10.3847/2041-8213/aba2cf)
- Nasa High Energy Astrophysics Science Archive Research Center (Heasarc). 2014, HEAsoft: Unified Release of FTOOLS and XANADU, Astrophysics Source Code Library, record ascl:1408.004. <http://ascl.net/1408.004>
- Olausen, S. A., & Kaspi, V. M. 2014, ApJS, 212, 6, doi: [10.1088/0067-0049/212/1/6](https://doi.org/10.1088/0067-0049/212/1/6)
- Scargle, J. D. 1998, ApJ, 504, 405, doi: [10.1086/306064](https://doi.org/10.1086/306064)
- Thompson, C., & Duncan, R. C. 1995, MNRAS, 275, 255, doi: [10.1093/mnras/275.2.255](https://doi.org/10.1093/mnras/275.2.255)
- van der Horst, A. J., Kouveliotou, C., Gorgone, N. M., et al. 2012, ApJ, 749, 122, doi: [10.1088/0004-637X/749/2/122](https://doi.org/10.1088/0004-637X/749/2/122)
- Younes, G., Güver, T., Kouveliotou, C., et al. 2020, ApJL, 904, L21, doi: [10.3847/2041-8213/abc94c](https://doi.org/10.3847/2041-8213/abc94c)
- Younes, G., Baring, M. G., Kouveliotou, C., et al. 2021, Nature Astronomy, 5, 408, doi: [10.1038/s41550-020-01292-x](https://doi.org/10.1038/s41550-020-01292-x)
- Younes, G., Hu, C.-P., Bansal, K., et al. 2022, ApJ, 924, 136, doi: [10.3847/1538-4357/ac3756](https://doi.org/10.3847/1538-4357/ac3756)
- Younes, G., Lander, S. K., Baring, M. G., et al. 2025, ApJ, 989, 89, doi: [10.3847/1538-4357/ade716](https://doi.org/10.3847/1538-4357/ade716)